



**Department of Earth Sciences**  
Halifax, Nova Scotia  
Canada B3H 4J1  
(902) 494-2358  
FAX (902) 494-6889

DATE: April 27, 2010

AUTHOR: Matt F. P. Abram

TITLE: Gas Hydrate Distribution and Volume at  
Sackville Spur

\_\_\_\_\_

\_\_\_\_\_

Degree: Honours B.Sc. Convocation: May 2010 Year: 2010

Permission is herewith granted to Dalhousie University to circulate and to have copied for non-commercial purposes, at its discretion, the above title upon the request of individuals or institutions.

Signature of Author

THE AUTHOR RESERVES OTHER PUBLICATION RIGHTS, AND NEITHER THE THESIS NOR EXTENSIVE EXTRACTS FROM IT MAY BE PRINTED OR OTHERWISE REPRODUCED WITHOUT THE AUTHOR'S WRITTEN PERMISSION.

THE AUTHOR ATTESTS THAT PERMISSION HAS BEEN OBTAINED FOR THE USE OF ANY COPYRIGHTED MATERIAL APPEARING IN THIS THESIS (OTHER THAN BRIEF EXCERPTS REQUIRING ONLY PROPER ACKNOWLEDGEMENT IN SCHOLARLY WRITING) AND THAT ALL SUCH USE IS CLEARLY ACKNOWLEDGED.

**GAS HYDRATE DISTRIBUTION AND VOLUME AT SACKVILLE SPUR**

**Matt E.P. Abram**

**Submitted in Fulfillment of the Requirements  
for the Degree of Bachelor of Sciences, Honours  
Department of Earth Sciences  
Dalhousie University, Halifax, Nova Scotia  
April 2010**

## Abstract

Natural methane gas hydrate in Canada's offshore continental margin represents a potential massive storehouse of naturally occurring crystalline methane formed under specific pressure-temperatures regimes. Natural gas hydrate is a crystalline substance composed of water and natural gas (commonly CH<sub>4</sub>) that forms in Arctic permafrost and offshore continental slope environments. Recognition of gas hydrate is continuing to evolve as a potential energy resource, a possible greenhouse gas contributor, and as a geohazard. The objective of this thesis is to estimate the volume of methane gas hydrate at Sackville Spur; a tapering sediment ridge formed under influence of the Labrador Current, a shallow-water ocean current that transports cold water from Baffin Bay in the North Atlantic southwards, roughly paralleling the continental shelf break offshore Newfoundland and Labrador. The presence of gas hydrate at Sackville Spur is inferred by the existence of a high-amplitude, phase-reversed BSR roughly 156km<sup>2</sup> in size. Two wide-angle reflection profiles at Sackville Spur were depth-converted using an averaged OBS velocity model to determine the depth of the BSR; found to range from 1280 – 1400 m below sea level. Sediment mineralogy approximations, derived from piston core data, suggest a mixture of 39% clay, 27% quartz, and 34% calcite. Effective medium modeling by fitting velocity gradients influenced by hydrate existence yields 9% hydrate concentrations at Sackville Spur, and estimated total hydrate volume of 1.12x10<sup>9</sup> m<sup>3</sup>.

Key Words: Sackville Spur, gas hydrates, bottom simulating reflector, ocean-bottom seismometer, hydrate stability

## TABLE OF CONTENTS

ABSTRACT	i
TABLE OF CONTENTS	ii
TABLE OF FIGURES	iv
TABLE OF TABLES	v
TABLE OF ABBREVIATIONS	vi
ACKNOWLEDGEMENTS	vii
CHAPTER 1: INTRODUCTION	1
1.1 Methane Gas Hydrate	1
1.2 Location of Study	3
1.3 Thesis Objectives	5
CHAPTER 2: GEOLOGIC SETTING	7
2.1 Geologic Setting & Glacial History	7
2.2 Sediment Drift Deposits	9
CHAPTER 3: METHANE GAS HYDRATE	13
3.1 Global Distribution	13
3.2 Global Importance of Gas Hydrate	14
3.2.1 As an energy resource	14
3.2.2 As a greenhouse contributor	16
3.2.3 As a geohazard	17

3.3	Hydrate Properties	18
3.3.1	Chemistry and classification	18
3.3.2	Gas hydrate stability zone	20
3.3.3	Detecting hydrate: <i>BSRs</i>	24
CHAPTER 4: ANALYTICAL METHODS		29
4.1	Data Acquisition	29
4.2	Velocity Model Analysis & Depth Migration	30
4.3	Piston Core Analysis	38
CHAPTER 5: RESULTS		40
CHAPTER 6: DISCUSSION		42
6.1	Velocity Model & Depth Sections	42
6.2	Comparison of Porosity Models & Gas Hydrate Concentrations	43
CHAPTER 7: CONCLUSIONS		46
REFERENCES		47
APPENDIX A		A1
APPENDIX B		B1

## TABLE OF FIGURES

Figure 1.1	Global inventory of natural gas hydrate	2
Figure 1.2	Study location & OBS, piston core location map	4
Figure 2.1	North Atlantic drift locations	9
Figure 2.2	Elongate contourite drift models	11
Figure 3.1	Arbitrary oceanic methane hydrate phase diagram	23
Figure 3.2	Theoretical velocity gradient diagrams	25
Figure 3.3	Seismic reflection profile lines, in TWT	27
Figure 3.4	BSR area map	28
Figure 4.1	OBS A, channel 1 alone Line 020	31
Figure 4.2	OBS velocity model, shown along Line 020	33
Figure 4.3	OBS velocity gradient	33
Figure 4.4	Average velocity gradient from OBS data	34
Figure 4.5	Applied velocity model to Line 021 & Line 020	36
Figure 4.6	Depth-converted seismic reflection profiles	37
Figure 4.7	CORE 14 porosity data with gradient	39
Figure 5.1	OBS velocity comparison to hydrate concentration curves	41

**TABLE OF TABLES**

Table I	Parameters for theoretical velocity model	39
---------	---	----

## TABLE OF ABBREVIATIONS

BSR	Bottom simulating reflector
OBS	Ocean-bottom seismometer
GHSZ	Gas hydrate stability zone
BGHSZ	Base gas hydrate stability zone
HVZ	High-velocity zone
LVZ	Low-velocity zone
MTD	Mass-transport deposit
GWP	Global warming potential
LPTM	Late Paleocene Thermal Maximum
NADW	North Atlantic Deep Water
TWT	Two-way travel time
NMO	Normal move-out
LWD	Logging-while-drilling
NPOR	Neutron porosity log
GSCA	Geological Survey of Canada – Atlantic
mbsl	metres below sea level

## ACKNOWLEDGEMENTS

I would like to thank my supervisor, Keith Loudon, for providing me with an interesting thesis topic to work on. Gas hydrates are now an intriguing potential energy resource play that I was unlikely to have studied in the absence of his expertise. I would also like to extend my gratitude to Calvin Campbell and David Mosher of the GSCA for, on numerous occasions, finding the time to discuss my work and for providing me with the data necessary to fulfill my objectives. Finally, the thesis could not have been completed without the software expertise of Helen Lau. Your assistance is greatly appreciated.

## CHAPTER 1: INTRODUCTION

### 1.1 Methane Gas Hydrate

Natural gas hydrates represent an enormous potential storehouse of ice-bound methane (CH<sub>4</sub>) in both onshore and offshore locations, capable of achieving concentrations up to 160 times greater than free gas (non-hydrate) when compared by mass in equal volumes (Majorowicz and Osadetz, 2003). Consequently, gas hydrate is generating widespread interest as a potential energy resource of the future. As a prospective natural gas play, porosity and permeability of hydrate-saturated sediment are important characteristics both in the on- and offshore. These characteristics vary in clastic reservoirs depending on lithology, grain size/mineralogy, compaction, hydration/de-watering, and cementation, and ultimately determine the volume and ability of flow of contained methane gas. Porous sediment has the potential to contain high concentrations of hydrate in a variety of crystalline forms, and will undoubtedly represent the focus of exploration efforts in the future.

Natural methane gas hydrate occurs in both Arctic permafrost and oceanic sediments around the world. Canada boasts a high potential for hydrate due to its position geographically. Extensive permafrost areas in the Arctic, and vast continental shelf regions in the offshore provide great potential for methane hydrate crystallization within Canadian borders. The position of inferred and confirmed hydrate deposits in both Canada and around the world are highlighted in Figure 1.1. The formation of gas hydrate depends on a number of factors, including the sediment grain size, sediment porosity, pressure, and temperature. Coarse-grained sediments commonly contain hydrate as pore fillings and disseminated grains, whereas

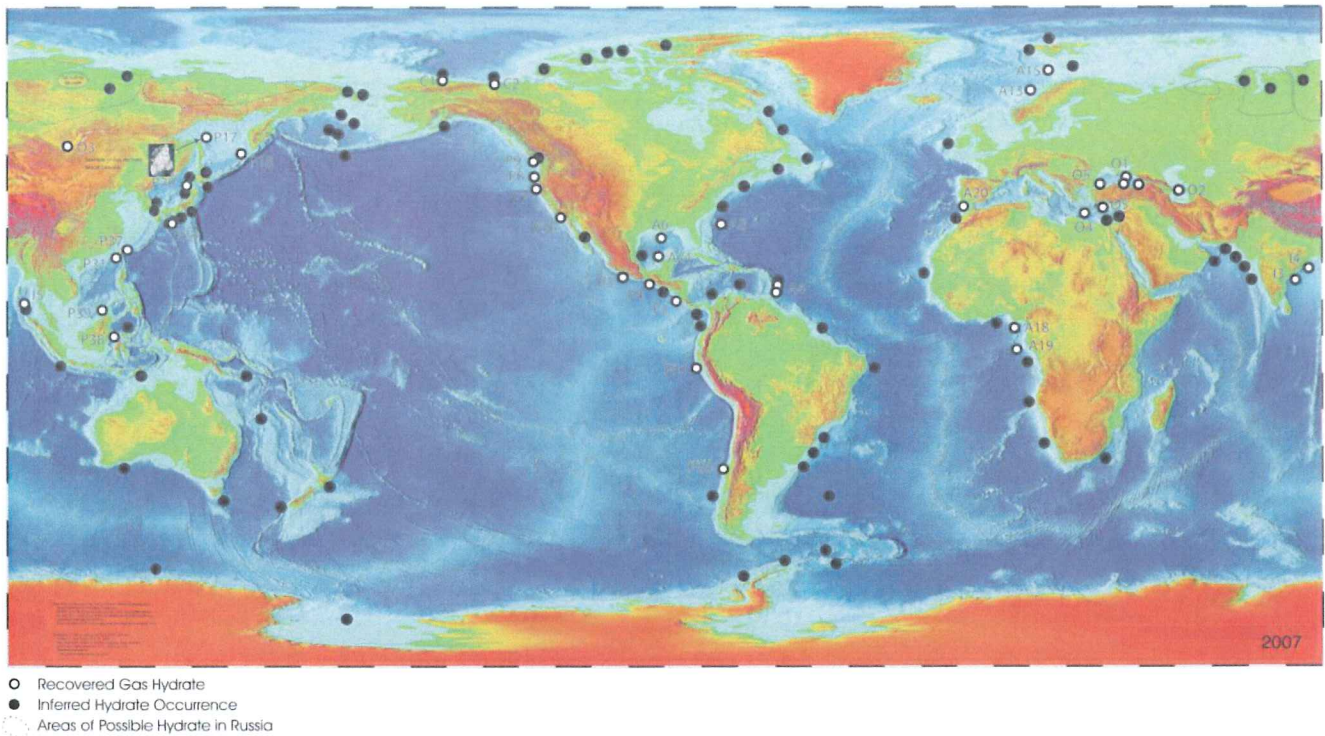


**Figure 1.1:** global inventory of natural gas hydrate. (modified from Kvenvolden and Lorensen, 2007)

fine-grained sediments display hydrate nodules and veins (Dillon and Max, 2000). The gas hydrate stability zone (GHSZ), or the subsurface sediment interval in which conditions are favourable for the formation of crystalline gas hydrate, is most influenced by pressure and temperature, as determined by water depth, bottom water temperature, overburden pressure, and geothermal heatflow.

In permafrost regions, low subsurface temperatures allow for a GHSZ that is stable relatively closer to the surface than for an oceanic equivalent. In northern Canada, bottom simulating reflectors (BSRs) identified in the onshore Mackenzie delta region led to the eventual confirmation of hydrate presence. On the Canadian Atlantic margin, hydrate is suspected to lie beneath the continental slope between water depths of 350 m and 3500 m (Mosher, 2008). The GHSZ varies markedly within oceanic

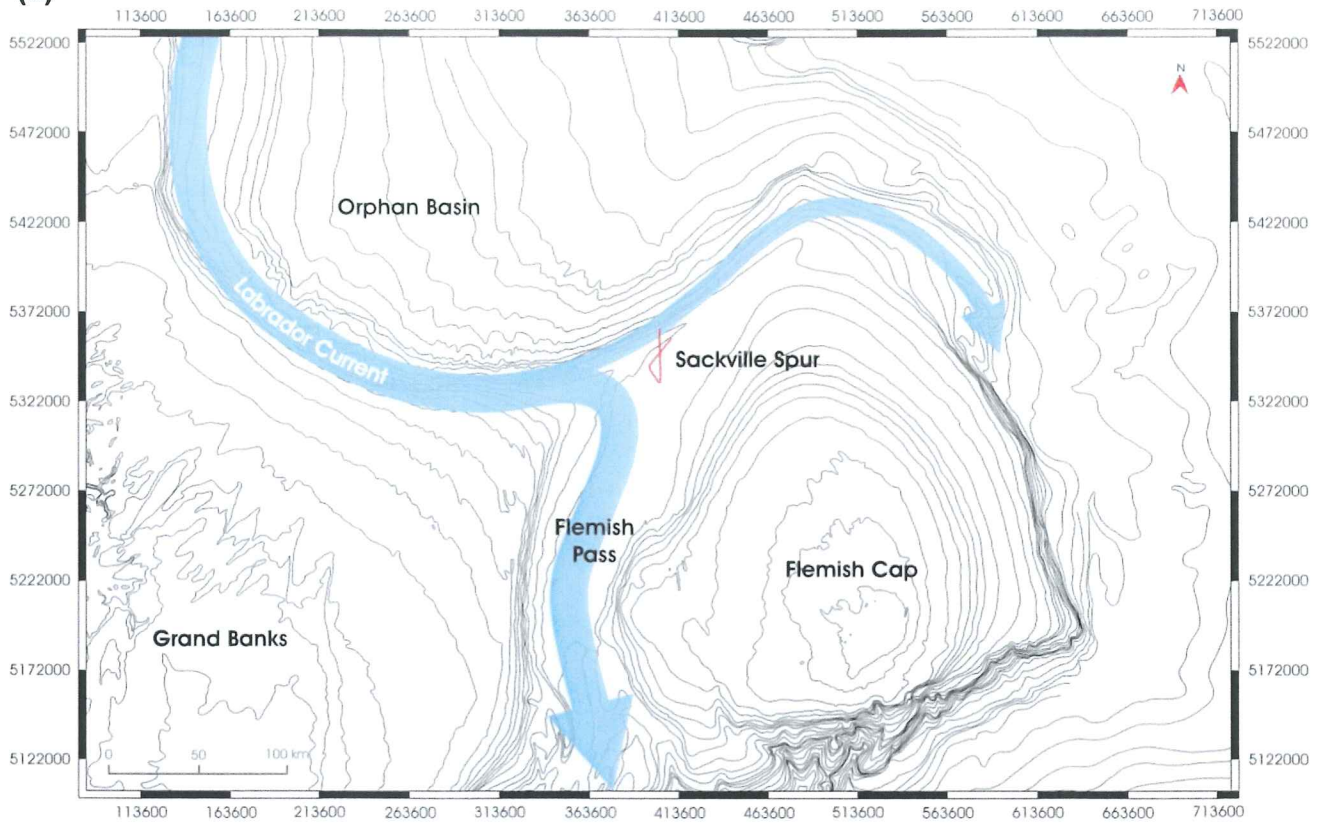
sediments, and is strongly influenced by bottom-water temperatures. For this reason, the GHSZ occurs at greater depths in the warm waters of the Mediterranean Sea than in the cold waters of the Arctic/North Atlantic.

BSRs are used to identify natural gas hydrate, including those observed in the Cascadia subduction margin offshore Vancouver Island, the onshore Mackenzie delta region, and along the offshore Atlantic margin. BSRs are a phase-reversed reflection event that is believed to represent the base of the GHSZ as a result of seismic velocity differences at the transition between the high-velocity ice-bound hydrate sediment and the underlying low-velocity free gas zone (Tucholke and Bryan, 1977). Methane gas is hypothesized to migrate through permeable subsurface beds to its position below the GHSZ, where further movement is restricted by the hydrate, thereby creating the phase reversed BSR. BSRs as indicators of hydrate are not bound by lithological boundaries or stratigraphic layers, but parallel the seafloor topography because they follow the stability isotherm. On the Labrador Shelf, the first prediction of gas hydrate (Taylor *et al.*, 1979) was based on hypothetical assumptions about the geothermal regime for ocean sediments, and low bottom-water temperatures in the Labrador Sea. At Sackville Spur, a series of high-amplitude dipping reflectors that signifies the presence of trapped free gas possibly represents the base of the hydrate stability field.

## 1.2 Location of Study

The Sackville Spur is an elongate sediment mound, also termed a sediment drift, located on the northeastern tip of the Grand Banks of Newfoundland, approximately

(a)



(b)

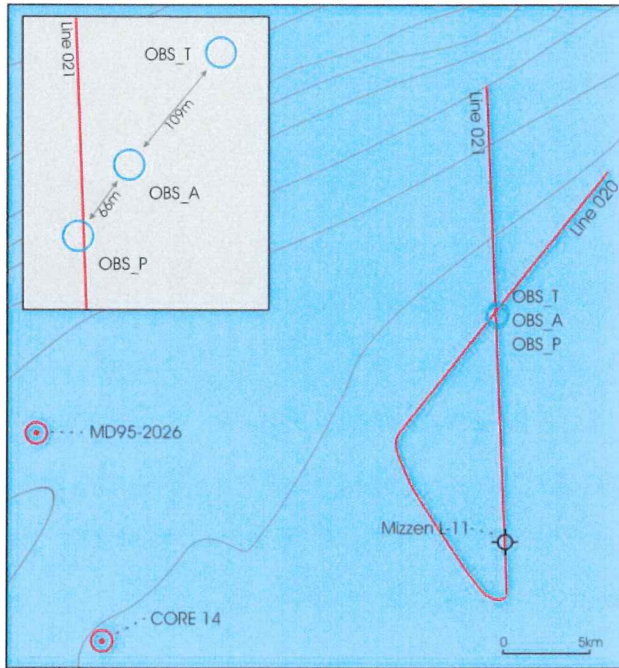


**Figure 1.2:** Study location map, displaying reflection surveys (Line 020, Line 021), and bathymetry contours. (a) At the spur, the cold-water Labrador Current (blue arrow) splits, forcing some waters eastwards, around Flemish Cap, while the majority of the current continues south, and is channelled through the 1200 m deep Flemish Pass. (b) Detailed map of Lines 021 and 020, with OBS and piston core positions plotted.

430 km offshore (Fig. 1.2). The spur forms a northeastwards-prograding sedimentary extension of the continental slope nearly 140 km long in water depths ranging from 1000 m – 2500 m (Kennard *et al.*, 1990). Sackville Spur is believed to have been formed by current-influenced deposition since the Late Miocene (approximately 8.4 – 9.2 Ma), during which time high glacial sediment input, and initiation of the southward-flowing Labrador Current developed conditions suitable for drift growth (Piper, 2005; Kennard *et al.*, 1990).

### 1.3 Thesis Objectives

Natural gas hydrate is believed to be present within the study area as indicated by the presence of subsurface BSRs, identified from two reflection lines (lines 020 & 021) recorded during CCGS Hudson cruise 2004-024 (Fig. 1.2). This thesis will aim to estimate the volume of methane hydrate present at the Sackville Spur BSR location by examining compressional (*p*-wave) velocity gradient variations caused by the existence of hydrate. A model by Helgerud *et al.* (1999) will be used to generate a series of velocity gradients at varying hydrate concentrations by assuming the effect of hydrate formation to be a simple reduction in porosity. In this model, hydrate is believed to become a strengthening component of the ocean bottom sediment, and ultimately affect compressional velocities as they relate to hydrate saturation. The output *p*-wave gradient will then be compared to the velocity model derived from three ocean-bottom seismometers (OBS) at the BSR location to provide an estimate of hydrate volume. It is hypothesized that the presence of hydrate above the BSR will increase *p*-wave velocities relative to the overall gradient of hydrate-free sediment at the OBS location.

The *confirmed* presence of gas hydrate at the study area is unlikely without drilling, and low concentrations may not be represented as a result of limited seismic detection resolutions.

In addition to the two seismic reflection profiles, physical property data of two piston cores retrieved from Sackville Spur will be examined (Fig. 1.2). These cores (MD95-2026 and CORE 14) will provide both mineralogical and porosity gradient approximations necessary for use in the hydrate velocity model developed by Helgerud *et al.* (1999).

This thesis will begin by generalizing the glacial history of the Grand Banks of Newfoundland, and highlight the important role of glacier-related sedimentation in the development of Sackville Spur. A summary of the characteristics of sediment drift deposits of the North Atlantic will be discussed in Chapter 2. Chapter 3 will focus on methane hydrate by providing insight into its global distribution and importance, chemical and physical properties, and geophysical detection methods. Analytical methods will be discussed in Chapter 4, and will provide a framework of analysis steps involved to complete this thesis. This will be followed by a summary of results and a discussion of their implications in Chapters 5 and 6, respectively. Conclusions and an estimate of the in-situ hydrate volume at Sackville Spur will be formulated in Chapter 7.

## CHAPTER 2: GEOLOGIC SETTING

### 2.1 *Geologic Setting & Glacial History*

The Grand Banks of Newfoundland, defined by the continental shelf characterized by several banks and channel systems in water depths no greater than 300 m, has an area in excess of 100,000 km<sup>2</sup> (Huppertz and Piper, 2009). Like most of the eastern Canadian, Norwegian, and Antarctic margins, the Grand Banks have been crossed repeatedly by glacial ice during major glacial stages (Warnke, 1970; Laberg and Vorren, 1995; Huppertz and Piper, 2009). Sedimentation in the mid-to-high latitudes was highly influenced by such events, which deposited thick sediment successions seaward of ice streams that extended across the continental shelves (Laberg and Vorren, 1995; Huppertz and Piper, 2009). Repeated glacial progradation 400 km from the Newfoundland coast, across the Grand Banks and to the shelf edge, is documented by the presence of prominent seafloor till ridges in the Sackville Moraine complex (Huppertz and Piper, 2009). However, while sediment is commonly carried to the deeper abyssal plain on the rest of the Canadian Atlantic margin, on the Eastern Grand Banks, most is trapped on the floor of a perched basin of Flemish Pass (Huppertz and Piper, 2009).

Flemish Pass (Fig. 1.2) is a mid-slope basin in approximately 1000 m water depth that lies above a graben formed during rifting of the North Atlantic (Campbell *et al.*, 2002). The Pass is bounded to the west by the Grand Banks, and to the east by Flemish Cap, where Precambrian basement rocks are exposed on the seafloor at less than 300 m depth (King *et al.*, 1985; Piper and Campbell, 2005). Quaternary sediments have prograded eastwards from the Grand Banks to Flemish Pass via debris flows and

turbidity currents, as well as by ice-rafting (Piper and Campbell, 2005). Icebergs carried southwards by the shallow Labrador Current from Baffin Bay have altered seafloor topography on the Grand Banks by causing pits and scours along the shelf and upper slope.

During the last glacial maximum, it is believed that ice advance only reached the mid-shelf, before retreating from the area 15,000 years ago (Huppertz and Piper, 2009). Sedimentation on the Grand Banks significantly increased during these periods of widespread shelf-crossing glaciation (Piper, 2005), at which time large volumes of suspended sediments were transported to the slope edge and reworked by storm waves and shallow ocean currents. Large sediment volumes on the Grand Banks provided an effective medium which the shallow Labrador and North Atlantic Deep Water (NADW) Currents would eventually re-deposit as part of the mass-transport deposit (MTD) Sackville Spur.

Widespread drift development in the North Atlantic was strengthened by massive sediment input from glaciers. Above-average sedimentation rates during glacial periods provided potential for the development of sandier, less clayey deposits forming along continental shelf margins. Reworking by the Labrador and NADW Currents during the Quaternary produced the drift deposit at Sackville Spur and a variety of other contourite deposits in the North Atlantic. Figure 2.1 displays sediment drifts present in the Atlantic/North Atlantic.

## 2.2 Sediment Drift Deposits

Bottom currents, defined as persistent water-mass flows near the seafloor, have significant influence on seafloor topography because of their ability to re-suspend, transport, and/or ultimately control the deposition of sediments (Faugères and Stow, 2008). Such currents are present throughout the world's oceans and flow in response to major thermohaline and/or wind-driven circulation patterns; however, primary flow paths may be temporarily displaced by tides, seasonal changes, and/or migrating eddies. In general, their position in the water column is variable, occurring everywhere from the abyssal floor to mid-slope and upper-slope settings (Faugères and Stow, 2008). Figure 2.1 displays sediment drifts present in the North Atlantic.

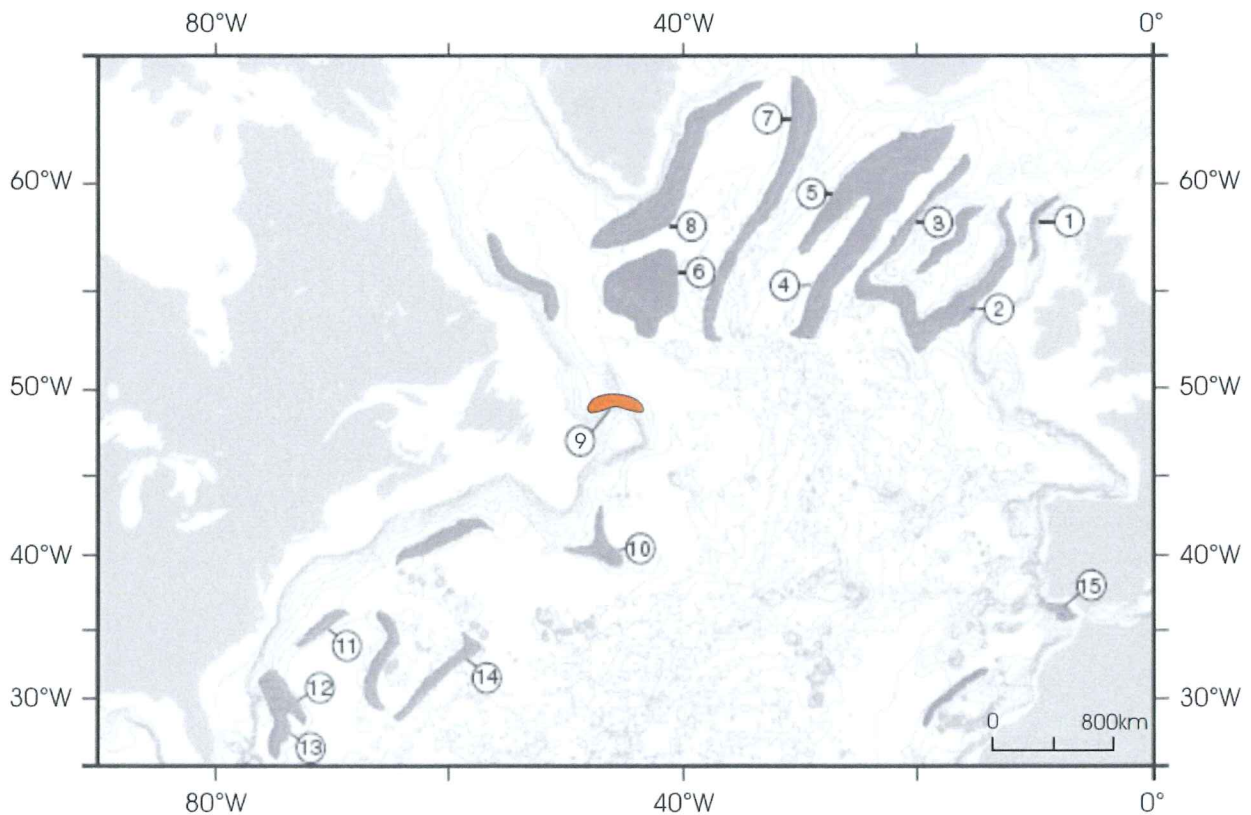


**Figure 2.1:** North Atlantic drift locations. Sackville Spur – 9; Blake Spur – 12; Bahama Spur – 13. (modified from Faugères and Stow, 2008)

The sediment deposits associated with bottom currents, referred to as *contourite drifts* or *spurs*, are primarily composed of current-deposited sediment of varying grain size and provenance. Glaciomarine sediment and associated turbidite and debris-flow deposits are also commonly associated with drift deposits on the seafloor, due primarily to slope instability as a function of constant sediment re-working (Faugères and Stow, 2008). The depositional processes involved in generating a sediment drift are not simple, and therefore it is relatively difficult to identify such a deposit through basic diagnostic criteria. Classification by depth is perhaps the most common, thereby subdividing contourites into i) deep-water (>2000 m), ii) mid-water (300 m – 2000 m), like that of Sackville Spur, and iii) shallow-water (<300 m) (Faugères and Stow, 2008). Due to the nature of contourite deposition, the size and shape of individual drifts is highly variable. Stow *et al.* (2002) identify five deposit types on a basis of shape and environment, of which Sackville Spur is best represented as an elongate drift (Fig. 2.2). Elongate drifts are dominantly asymmetric, characterized by steeply dipping upstream sides and less steep downstream sides as a function of dominantly erosive and depositional processes, respectively (Deptuck *et al.*, 2007).

Drift morphology is directly linked to current characteristics: the stronger the current, the coarser the sediment; the thicker the drift, the older the current activity (Viana and Rebesco, 2007). Current strength is derived from its speed, and has been noted to increase during glacial periods when intensified glacial bottom-water generation was facilitated by large ice volumes and greater cooling rates due to relative sea level lows.

## Type II - Elongate drifts

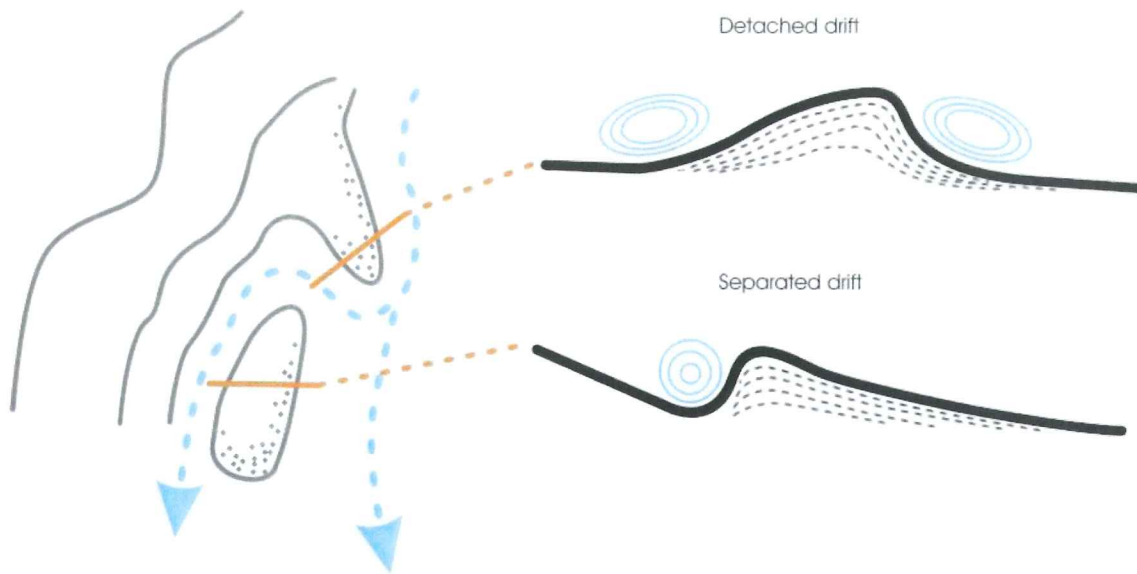


**Figure 2.2:** elongate contourite drift models. Sackville Spur is classified as an elongate drift, on the basis of geometrical similarities with drift types identified by Stow *et al.* (2002). (modified from Stow *et al.*, 2002)

Sackville Spur is a tapering sediment ridge under constant reworking by the Labrador Current, as it transports cold water from Baffin Bay in the North Atlantic southwards, roughly paralleling the continental shelf break offshore Newfoundland and Labrador. At Sackville Spur, the Labrador Current splits, thereby channelling the bulk of the current volume southwards through Flemish Pass, and the remaining volume further east, around Flemish Cap (Fig. 1.2).

The steep northern flank of Sackville Spur is inclined at  $3^{\circ}$ - $5^{\circ}$ , and plunges to the 2500 m deep floor of the Orphan Knoll basin. The southwards, downstream side dips gently at  $1^{\circ}$ - $1.5^{\circ}$  towards the southwest and the 1200 m deep Flemish Pass (Kennard *et al.*, 1990). Highly continuous reflections display prominent cross-beds composed of variable-coloured clay to silty- or sandy-clay, as suggested by piston cores (Deptuck *et*

*al.*, 2007). A prominent angular unconformity separating Middle Miocene sediments from overlying Early Pliocene sediments was identified, and likely corresponds with intensification in drift building as proglacial sediment plumes became available (Kennard *et al.*, 1990; Piper, 2005).

Failure scarps and over-steepening on the surface of the spur are believed to represent sediment failure a) under its own weight, b) by ground-shaking associated with earthquakes, or c) as a result of hydrate dissociation (Deptuck *et al.*, 2007). Small-scale growth faults, likely a result of current undercutting and drift over-steepening, have also been identified in the seismic sections (e.g. Fig. 3.3 (a)).

## CHAPTER 3: METHANE GAS HYDRATE

### 3.1 *Global Distribution*

Natural gas hydrate represents a massive potential storehouse of crystalline methane. Modest estimates suggest that hydrate volumes on Earth may exceed 10 terratonnes ( $10^{19}$  g) of ice-bound methane (Kvenvolden and Lorenson, 2001) in both permafrost and oceanic sediments: a figure representing nearly double the total volume of all other known hydrocarbons on the planet (Max, 2000). However, it is suggested that such estimates are generally poorly quantified and probably exaggerated; a consequence of assuming the maximum migration and trapping potential of total produced methane gas, in addition to the assumption that the temperature-pressure regime at the trap location is favourable to methane hydrate formation. Gas hydrate is distributed globally in two common locales: the permafrost sediments of Arctic regions, and the continental slope sediments in the offshore. At these locations, the appropriate pressure-temperature regimes exist that allow hydrate formation. Due to the goal of this thesis, oceanic hydrate is of primary interest, and therefore continental hydrate will only be discussed for comparative purposes.

Hydrate presence in the offshore likely exists in continental margins for several reasons, including: 1) the ocean margins are where the flux of organic matter is greatest due to a high rate of biological productivity, and a relative clustering of organic detritus as it is 'washed' from the continents, and 2) sedimentation rates are fastest here, ultimately covering and sealing the organic matter before it is oxidized (Dillon and Max, 2000). In such reducing environments, bacteria are able to feed off the organic detritus

and produce methane gas that, under appropriate conditions, will combine with host water molecules and facilitate hydrate crystallization.

The amount of hydrate in ocean sediments is possibly immense and widely distributed, but like almost every natural resource that is extracted for human use, commercial production would only be pursued at sites of naturally high concentrations. Methane hydrate has been discovered in almost every location along the continental slope that has been intensively explored (Dillon and Max, 2000). However, like oil and gas exploration, global oceanic hydrate presence mapped by those like Kvenvolden and Lorensen (2007) identify areas of high concentrations where the dominant method of geophysical surveys have provided a resolution fine enough to image subsurface deposits. There is no doubt hydrate exists in vast amounts, the challenge is to detect it. Presently, there is no commercial hydrate production.

## 3.2 *Global Importance of Gas Hydrate*

### 3.2.1 *As an energy resource*

Projected hydrate volumes discussed in *Section 3.1* demonstrate the energy potential of methane hydrate; especially when methane mass in hydrate can amount 160 times that of conventional natural gas reservoirs (Majorowicz and Osadetz, 2003). When burned, gaseous methane produces less CO<sub>2</sub> per unit of energy than any other fossil fuel (Bil, 2000), and has the potential to develop as a future energy resource, as global energy demand continues to grow and conventional sources decline. Oceanic hydrate is currently less favoured for development compared to continental hydrate, due largely to operational logistics, technological availability, and cost. Low pore filling

percentages and lengthy formation times classify gas hydrate as a non-renewable energy resource.

Methane production from hydrate is a process yet to be pursued at a commercial scale, but may eventually tap the natural gas potential stored in hydrate deposits around the world. To produce methane in its gaseous state, the dissociation process must be induced to liberate methane from its crystalline host water molecule. The dissociation process is an endothermic chemical reaction, in which heat is required to break the van der Waals forces between the methane (guest) and host water molecules.

The primary issue associated with hydrate extraction, however, stems from its high operating costs, technological shortcomings, limited hydrate education, and restricted access in both on- and offshore regions. Sloan and Koh (2008) suggest that hydrate plays existing under ideal reservoir conditions in onshore permafrost environments would likely not prove economically viable until gas prices exceeded \$9/MMBTU (one hundred thousand British Thermal Units) (based on 2005 economics).

The Mallik well in the Mackenzie Delta in northern Canada is of particular interest. Well log determinations and core studies identified a gas hydrate deposit exceeding 110 m total thickness in an exploration well drilled by Imperial Oil Ltd. in 1971. Methane hydrate saturation values exceeding 80% of the pore volume have made the Mallik gas hydrate field one of the most concentrated hydrate reservoirs in the world (Dallimore and Collett, 2005). Recent production tests led to 6 days of continuous production; however, no prolonged commercial production is expected due to the lack of pipeline and production infrastructure in the area.

Technological complexities have also contributed to limited industry interest in hydrate production, particularly in the offshore where operating environments pose a much greater challenge. As a result, onshore permafrost hydrate is expected to first come online when a) the supply of conventional and unconventional gas is suspected to have begun to decline (Sloan and Koh, 2008), and b) technological advancements have been made to facilitate applications of hydrate production.

### 3.2.2 *As a greenhouse contributor*

Hydrate presence in sediment has a strong implication for climate change due to the immensity of the deposit volumes and the global warming potential (GWP) of methane in the atmosphere. Due in large part to greater estimated volumes in the offshore, hydrate dissociation in the oceans as a result of temperature, pressure, and chemical anomalies (discussed further in *Sect. 3.2.3* & *Sect. 3.3.2*) has the potential to release large volumes of gaseous methane into the atmosphere and exacerbate global warming.

Deep water CH<sub>4</sub> emissions are often oxidized/dissolved in the water column before reaching the atmosphere; however, methane released in shallow shelf settings has the potential to reach the atmosphere before being completely oxidized to CO<sub>2</sub>, thereby potentially influencing global climates. In the Arctic, hydrate dissociation may result from sea level rise, at which point flooding of the coastal plain permafrost sediment will force warming, and instability in the GHSZ. If temperatures surpass that of the critical hydrate temperature at that location, dissociation will occur and gaseous methane will be released to the shallow water column, and potentially to the

atmosphere. In the offshore, geologically instantaneous events like landslides can rapidly reduce overburden pressures in ocean sediments, and force dissociation. If hydrate volumes are large and relative water depths marginal, the potential exists for gaseous methane to escape the water column and pass into the atmosphere. Although methane will slowly be oxidized to CO<sub>2</sub> while in the atmosphere, the absorption properties of CH<sub>4</sub> are much different than that of CO<sub>2</sub>. As a result, the GWP of gaseous methane is calculated to be 56 times greater than that of CO<sub>2</sub> over a 20 year period (Dillon and Max, 2000).

The Late Paleocene Thermal Maximum (LPTM), occurring ~55M years ago, was a brief warming period hypothesized to have been caused by oceanic hydrate dissociation and the expulsion of massive volumes of gaseous methane into the atmosphere (Sloan and Koh, 2008). Over the next 10,000 years, global temperatures increased 4-8°C, as documented in measured deep ocean <sup>13</sup>C isotope drill samples (Sloan and Koh, 2008). Changing ocean circulation systems at the time are thought to have moved warm surface waters to depth, therefore inducing change in sediment geotherms and forcing hydrate dissociation. The LPTM is an important event because it is an analogue available in the geologic record that displays the effects on the global carbon cycle in relation to large hydrocarbon fluxes into the system.

### 3.2.3 *As a geohazard*

A variety of topographic features on the seafloor have been linked to dissociation of gas hydrate, including pockmarks and mass-wasting events. Pockmarks are crater-like features that are believed to represent gas escape features related to fault zones,

salt diapirs, and/or hydrate dissociation (Gay *et al.*, 2003). They generally occur in unconsolidated, fine-grained sediment as circular seafloor depressions with a maximum diameter of 300 m, and  $\leq 80$  m deep; although bottom tidal currents in the continental margin can cause elongation (Gay *et al.*, 2003; Ondréas *et al.*, 2005). Methane released to the water column in this fashion is caused by gas overpressure at depth.

Mass-wasting events associated with hydrate dissociation can also influence seafloor topography. Because it generally forms prior to lithification, crystalline gas hydrate can strengthen sediment, and therefore any significant variation in temperature-pressure conditions has the potential to force dissociation, and the loss of sediment rigidity (Max, 2000). The Newfoundland continental slope has undergone a series of significant mass-failures in which hydrate dissociation may have been a contributing factor (Mosher, 2008). Slope stability is an important concern in hydrocarbon exploration efforts in the offshore. In addition, large-scale events, a result of increased pore fluid pressures by hydrate dissociation, have the potential to develop into geohazards (e.g. tsunamis).

### 3.3 *Hydrate Properties*

#### 3.3.1 *Chemistry and classification*

Natural gas hydrate is a crystalline substance composed of water and natural gas that can form in high pressure – low temperature regimes in polar regions and oceanic sediments. The host water molecules are arranged in a framework of rigid cages (known as a clathrate) that are stabilized by occupant guest molecules; commonly methane (CH<sub>4</sub>). The stability of oceanic clathrates is dependant on pressure,

temperature, activity of the water, and gas concentration. The 100% methane hydrate stability zone is modelled by *Equation 3.1*, where  $T_{St\_100}$  is the temperature of stability ( $^{\circ}\text{C}$ ), and  $D$  is depth (m), converted from pressure by assuming a linear hydrostatic gradient of 10 MPa/km in the water column and the sediments (Majorowicz and Osadetz, 2003).

$$T_{St\_100} = 8.9m(D) - 50.1 \quad (3.1)$$

Methane hydrate is classified in terms of crystal structure and gas origin, and occurs as either Type I or Type II. Type I methane hydrate is nearly pure, containing 99% methane and trace amounts of  $\text{H}_2\text{S}$  and  $\text{CO}_2$ . This type of methane hydrate is believed to have a biogenic origin; a product of the methanogenesis process, by which methane gas is created in shallow oceanic sediments as a function of organic  $\text{CO}_2$  reduction. Analyzed Type I hydrate samples generally display carbon-isotope compositions lighter than that of  $-60\text{‰}$  (i.e. more positive than  $-60\text{‰}$ ), indicating they have been a) generated in place, b) migrated short distances, or c) naturally recycled as a function of continued sedimentation (Kvenvolden and Lorenson, 2001).

In contrast, Type II hydrate is characterized by the presence of ethane, propane, and other long-chain molecules in addition to methane, and is believed to have a thermogenic origin; a product of thermal decomposition of organic matter at depths exceeding 1000 m (Kvenvolden and Lorenson, 2001). Type II hydrate is quite rare, and is heavier than  $-60\text{‰}$  (i.e. more negative than  $-60\text{‰}$ ), and is stable at higher temperatures (Kvenvolden and Lorenson, 2001). The bulk of proven gas hydrate occurrences are Type I, but Type II hydrates have been identified in the Gulf of Mexico, Mackenzie Delta, and Caspian Sea. With respect to conventional petroleum systems,

Type I hydrate would likely represent primary targets due to its inherent richness in CH<sub>4</sub>, and relative low abundance of unwanted guest molecules in the clathrate (i.e. H<sub>2</sub>S).

Hydrate presence in offshore sediment has also been examined by McConnell and Kendall (2002). Their findings suggest unique crystal structures in Type I and Type II hydrate. Type I commonly exists as discrete and dispersed nodules within the sediment; whereas massive deposits characterize Type II as a product of large volumes of thermogenic gas migrating upwards from depth.

Hydrate formation within the sediment column mainly results in its strengthening. As a function of the frame bulk modulus, or rigidity of the clathrate structure, the physical and acoustic properties of the sediment are increased with increasing hydrate concentration (Lee and Collett, 2001). Compressional wave velocities may increase from 1.6 km/s in normal sediment to 2.5 km/s or higher in hydrated sediment. Shear wave velocity increases have also been noted.

### *3.3.2 Gas hydrate stability zone*

The GHSZ defines the subsurface sediment interval in which conditions are suitable for the formation of crystalline gas hydrate. It is most influenced by pressure and temperature; variables affected by water depth and overburden pressure, bottom water temperature and the geothermal gradient, respectively. In the presence of methane saturation and available sediment porosity, hydrate has the potential to form if a high pressure – low temperature regime exists. In Arctic permafrost sediments, shallower hydrate deposits (generally 150 m below the surface) have been confirmed as

a direct result of colder temperatures near the surface (Kvenvolden *et al.*, 2000). Hydrate would not usually be found that close to the surface, however, Arctic climates provide low temperatures necessary to shift the geothermal gradient, and facilitate hydrate crystallization. Oceanic hydrate, on average, occurs at water depths >300 m, at which point bottom water temperatures are low enough to facilitate hydrate formation (refer to Fig. 3.1) (Kvenvolden and Lorenson, 2000). On the Canadian Atlantic margin, the stability zone lies beneath the continental slope at depths between 350 m and 3500 m (Mosher, 2008).

Hydrate can crystallize at any depth in the GHSZ, including just below the seafloor. However, like ice, the density of crystalline methane hydrate is less than that of water (approximately  $0.9 \text{ kg/m}^3$ ) (Dillon and Max, 2000). This means that if hydrate formed in the water column or within the pore space of poorly consolidated sediments, it is possible for it to float upwards and dissociate when it crosses the methane phase boundary, shown in Figure 3.1. For this reason, shallow seafloor sediments do not commonly contain hydrate due to their unconsolidated nature and inability to preserve significant concentrations of methane that are favourable for hydrate crystallization. In special cases, hydrate can exist close to the seafloor. On the Cascadia Margin offshore Vancouver Island, hydrate was confirmed from piston cores taken at depths 3 – 8 m below the seafloor (Riedel *et al.*, 2002).

Hydrate chemistry, discussed previously in *Section 3.3.1*, also has a profound influence on the depth of the GHSZ, and results in varying stability characteristics for Type I & II methane hydrate. The GHSZ of Type I hydrate can be generalized to exist at a shallower subsurface interval compared to Type II hydrate. In locations like the

Gulf of Mexico, where methane gas is accompanied by other long-chain molecules like ethane and propane, the GHSZ has been noted to occur at greater sediment depths (at a pressure equivalent of 2.5 km). Studies performed by Dillon and Max (2000) suggest that the base of the GHSZ (BGHSZ) in the 2500 m deep waters of the Gulf of Mexico will occur at about 21°C (294°K) for pure methane, or 23°C (296°K) for a typical mixture of approximately 93% methane, 4% ethane, and 1% propane. However, at the same depth/pressure, a common Type II mixture of approximately 62% methane, 9% ethane, and 23% propane will have a BGHSZ that occurs at 28°C (301°K); signifying an increased depth of the BGHSZ.

A sandy lithology is an important reservoir for natural gas hydrate, by providing maximum permeability and porosity potential for methane migration and hydrate formation. Accordingly, the sandy character of the Gulf of Mexico has been estimated to contain

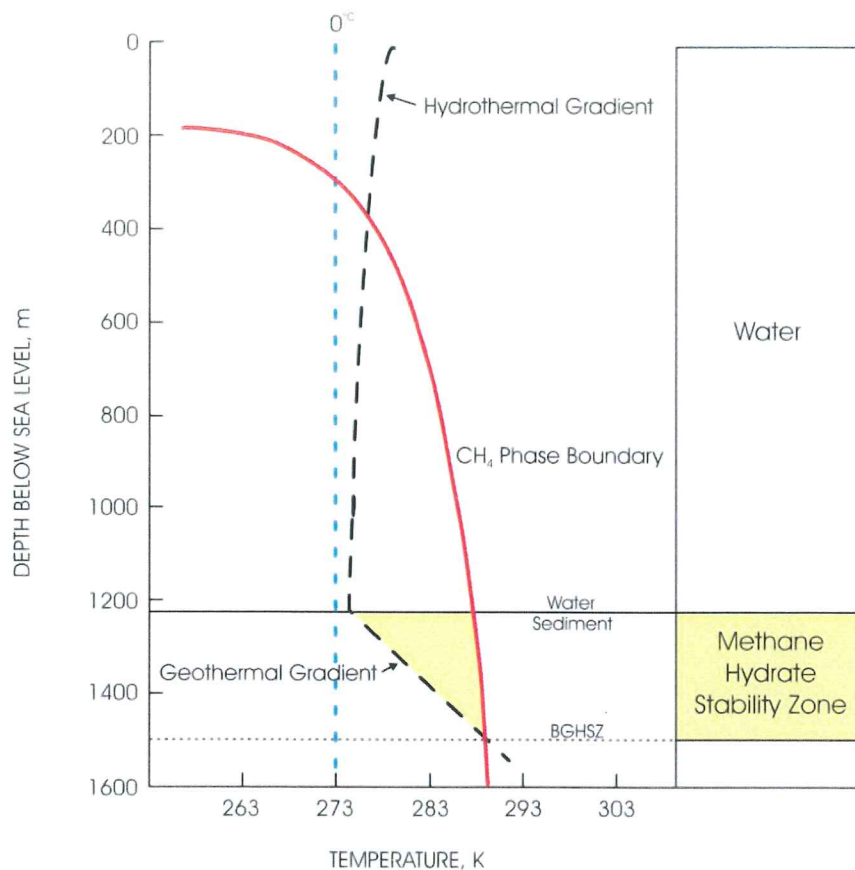


**Figure 3.1:** Arbitrary example of oceanic methane hydrate phase diagram. Oceanic gas hydrate will only form in sediment where the appropriate temperature and pressure regime exists. The depth at which the geothermal gradient crosses the methane phase curve marks the base of the GHSZ (BGHSZ), where temperatures are too warm for hydrate crystallisation. Below the BGHSZ methane gas and water will be stable, but methane hydrate will not. (modified from Max (ed.), 2000)

volumes of hydrate greater than that of the characteristic silty-clay sediment of the Blake Bahama Ridge, offshore Florida in the Atlantic Ocean (Sloan and Koh, 2008).

Changes in the stability field of the GHSZ are caused by temperature, pressure, and chemical anomalies of a variety of types. Fault-related warm fluid circulation (increasing formation temperatures beyond hydrate stability) and salt diapirism (characterized by dissolved salt ions essentially acting as inhibitors to hydrate formation) can force gradual temperature increases within the sediment, and alter the position of the GHSZ through dissociation. Salt is a very effective heat conductor that

can force changes in the thermal gradient, and be the cause of dissociation. Pressure variations associated with tectonic forces, sea level change, and mass-movement events can also alter the position of the GHSZ. Landslides, that remove overlying sediment and expose formerly deeper sediment containing the GHSZ, are relatively instantaneous events that ultimately reduce pressures, and may be linked to periods of immense hydrate dissociation (Sloan and Koh, 2008).

### 3.3.3 *Detecting hydrate: BSRs*

Geophysical surveys are the most effective methods to identify natural gas hydrate in on- and offshore regions. A bottom simulating reflector, or BSR, is a phase-reversed reflection event that is believed to represent the BGHSZ, or the top of the free gas zone, as a result of a sudden seismic velocity contrast at the transition between the high-velocity ice-bound hydrate sediment and the underlying low-velocity free gas zone (Tucholke and Bryan, 1977). Therefore, a BSR is a reflection event at the transitional boundary between, a) gas hydrate and methane gas, b) gas hydrate and sediment, or c) methane gas and sediment (Fig. 3.2).

As a function of hydrate stability, BSRs do not appear to be bounded by lithological boundaries, but rather roughly parallel the seafloor, often increasing in sediment depth with increasing water depth (Kvenvolden and Lorenson, 2001). Because the GHSZ is more sensitive to temperature changes than pressure changes, the BGHSZ, which defines a BSR, follows sediment isotherms which approximate the shape of the seafloor. Despite the fact that roughly 90% of all sea-floor sediment exists in hydrate-favourable temperature-pressure regimes, BSR occurrences are seemingly

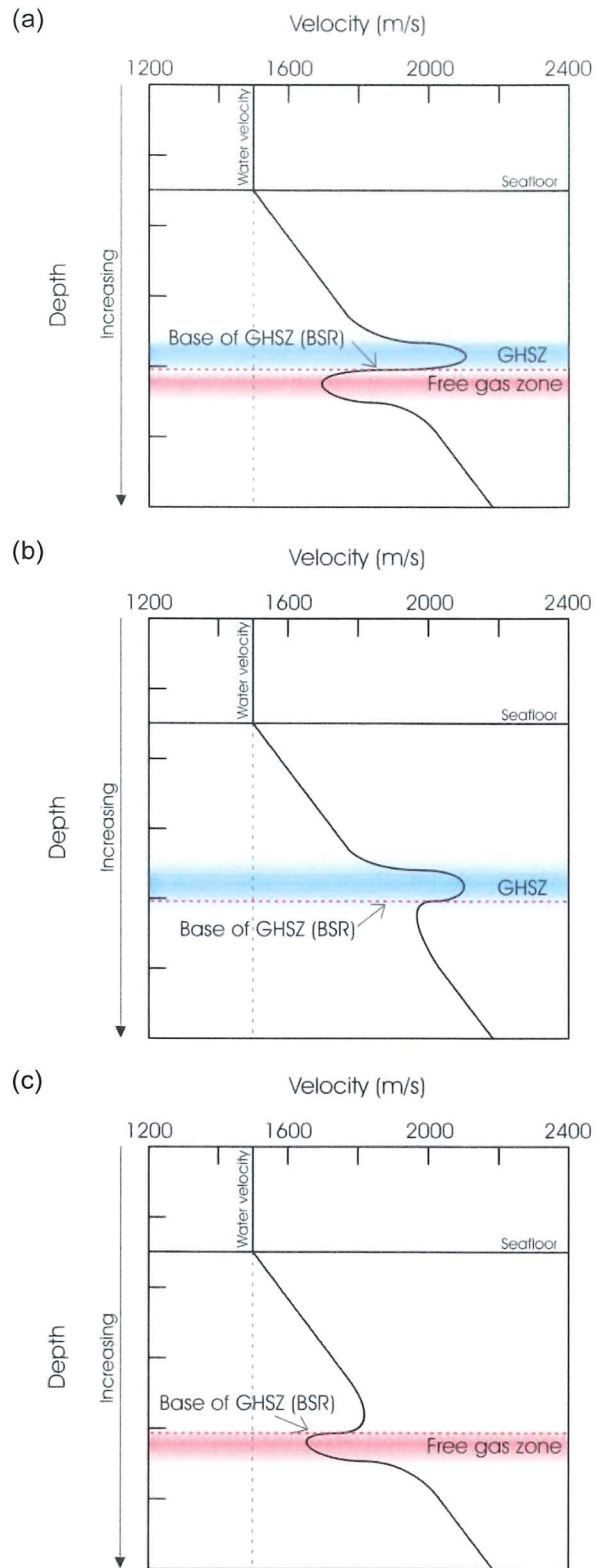


**Figure 3.2:** Theoretical velocity gradient diagrams. Velocity inversion caused by (a) gas hydrate and free gas; (b) gas hydrate only; and (c) free gas only.

limited to continental slopes and insular margins in global oceanic regions where the abundance of free gas is high enough to be detected and imaged by geophysical surveys (Kvenvolden and Lorenson, 2001).

Further indirect evidence of gas hydrate presence is provided by negative Cl<sup>-</sup> anomalies in sediment pore fluids. Such chloride anomalies result from the release of hydrate water during core retrieval with the dilution of the normal pore water chlorinities (Hesse, 1990). Direct retrieval of gas hydrates to the surface is a challenging task that requires *in situ* conditions be maintained throughout the extraction process. If conditions change, Cl-depletions of up to 20% (relative to mean seawater chlorinity) have been noted at distinct hydrate horizons in the subsurface (Suess *et al.*, 2001).

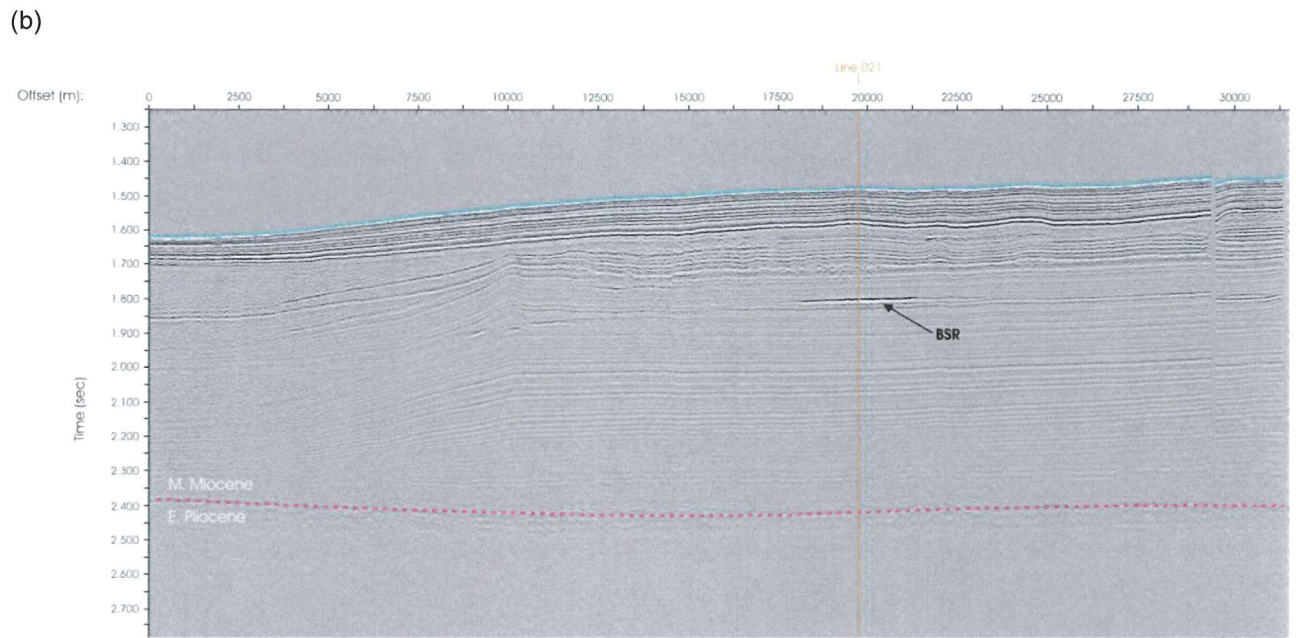
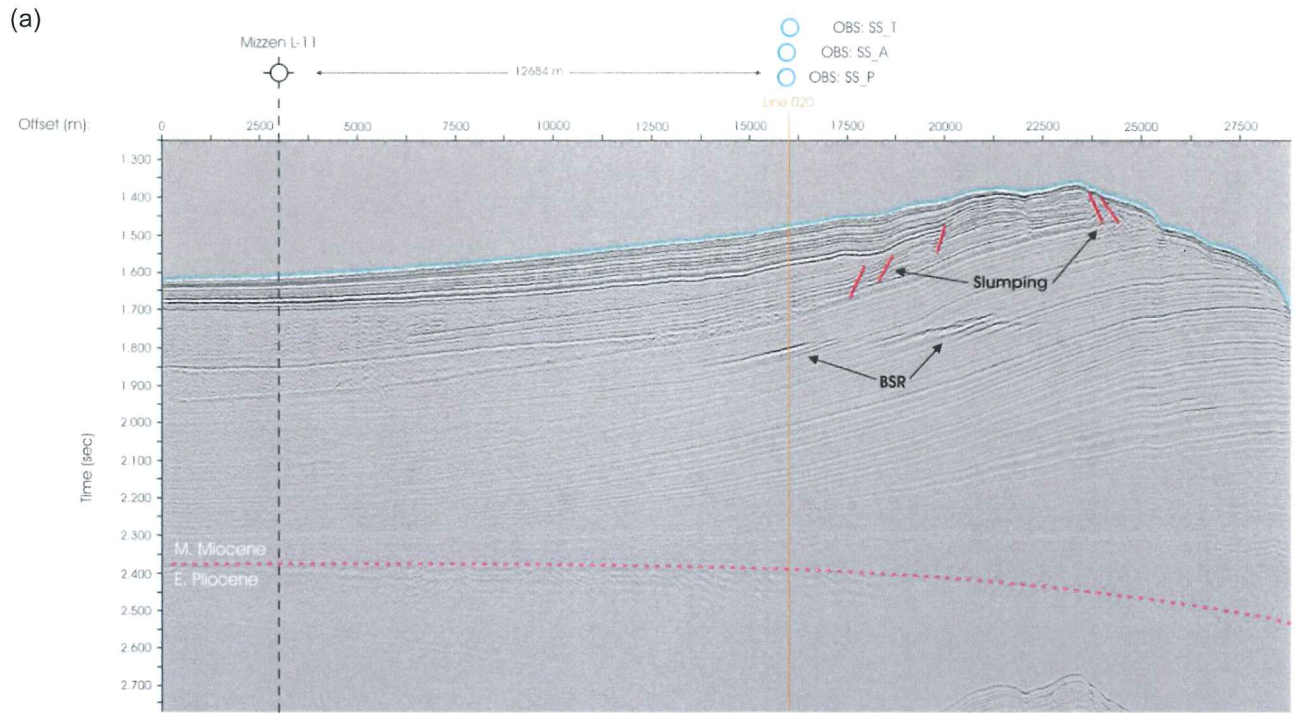


**Figure 3.3:** Subsurface BSRs imaged in TWT reflection profile lines (a) Hud2004-024-021 and (b) Hud2004-024-020. (a) Line 021, displaying a dipping BSR that appears to cut lithological boundaries and parallels the seafloor. The northern, steeply-dipping upstream side is dominated by erosive processes, whereas the southern, less-steep downstream side is dominated by sediment deposition. Small-scale growth faulting has been identified. (b) Line 020, displaying the BSR.

It is important to note that gas hydrate can occur without the formation of a BSR. BSRs are detectable in areas where free gas is trapped beneath hydrate. If there is no free gas zone, than no BSR will be imaged (Xu and Ruppel, 1999). The acoustic phase reversals that depict BSRs are caused by velocity contrasts in free gas and hydrate, thereby providing an impedance contrast that is imaged as a subsurface reflection boundary.

A BSR imaged at Sackville Spur is a series of brightened, high-amplitude reflectors that dim-out at 320 – 360 ms below the seafloor (Mosher, 2008). In map view, these brightened amplitudes define an area as least 156 km<sup>2</sup> in size, shown in Figure 3.4, below (Mosher, 2008). This area provides a rough approximation of the extent of gas hydrate at Sackville Spur (under the assumption that hydrate exists above the BSR), and will be necessary to fulfill the final goal of estimating hydrate volumes at the Spur.

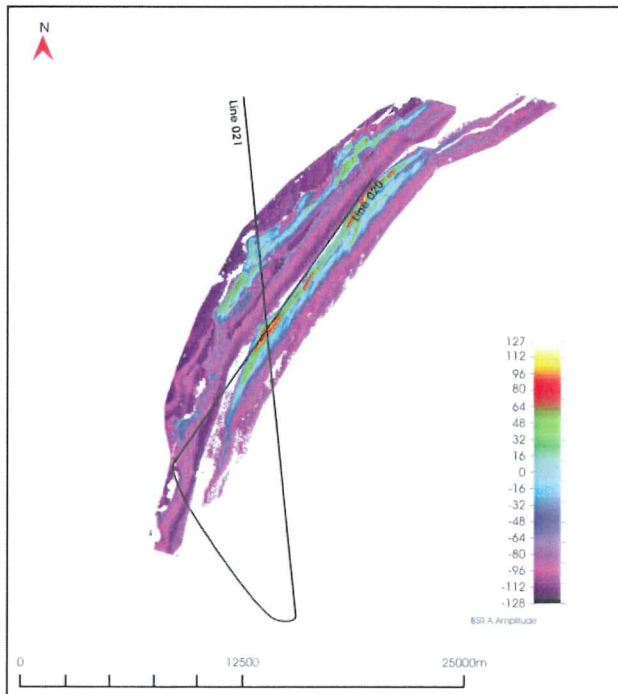


**Figure 3.4:** BSR area map. Large negative amplitudes defining the subsurface BSR at Sackville Spur.

## CHAPTER 4: ANALYTICAL METHODS

### 4.1 Data Acquisition

Three OBS (P, A, and T) were deployed to the seafloor at the mid-point of the two reflection profiles (Fig. 1.2). They were positioned above a subsurface BSR that had previously been identified from the *Geological Survey of Canada – Atlantic (GSCA)* and industry reflection profiles with a purpose of determining the velocity structure of the upper sediments and any anomalies associated with the existence of gas hydrates. The resulting reflection profiles, shown previously in Figure 3.3, and velocity analyses were provided by the GSCA for use in this thesis.

Physical property data from two piston cores retrieved from Sackville Spur were also examined (Fig. 1.2). The Marion Dufresne Core (MD95-2026) is a 25 m core collected in 1995, and is located approximately 28 km west of the OBS position. Mineralogical data from this core will provide estimates necessary for use in the hydrate velocity model developed by Helgerud *et al.* (1999). The second core, Core 14, was retrieved during Hudson Cruise 043 in 2001. It is 10 m in length, and is located approximately 29 km southwest of the OBS position. Physical property data of Core 14 will be used to generate a local porosity gradient assumed to be identical at the OBS location.

The Mizzen L-11 well was the first Petro-Canada, Flemish Pass, deepwater oil exploration well drilled in 2003. It is located along profile Line 021, roughly 484 km east-northeast of St John's, Newfoundland (Fig. 1.2). Deep gas targets were unsuccessful, and the well was abandoned. A series of wireline and logging-while-drilling (LWD) logs were run at the well location, and were examined for potential use in

conjunction with the core data to provide a strengthened approximation of the porosity and velocity models.

#### 4.2 Velocity Model Analysis & Depth Conversion

Determining the volume of methane hydrate at Sackville Spur is heavily dependant on the velocity model used to represent  $p$ -wave velocities within the sediment at depth. Dr. Deping Chian, under contract to the GSCA, developed a velocity model by fitting travel time curves from a velocity-depth model to the observed reflectors and refractors imaged by the three (3) OBS devices at the study location. The gradient of each velocity layer will differ based on its properties (i.e. density (compaction), water saturation, etc.) as well as the overall velocity gradient. Velocities were primarily constrained by the move-out of the reflected arrivals recorded by the OBS. However, because reflections are more sensitive to depth, and refractions to velocities, a more accurate model could be developed by ray tracing both, and using refracted arrivals to reinforce the accuracy of the gradient (LeBlanc *et al.*, 2007).

Figure 4.1 displays reflection and refraction ray traces, after travel time normalization was applied to flatten the seafloor. Refracted arrivals appear above the seafloor as a result of increased velocities at depth. Acoustic reflections 'bounce' off subsurface boundaries due to impedance contrasts at the contact of two unique mediums. Refractions, however, 'bend' through subsurface units as a function of physical property changes before returning to the surface. As a result, the travel time of refracted  $p$ -waves can be significantly decreased while travelling through high velocity

layers at depth, and can potentially result in recording times less than those of even direct waves (in the case of long receiver arrays).

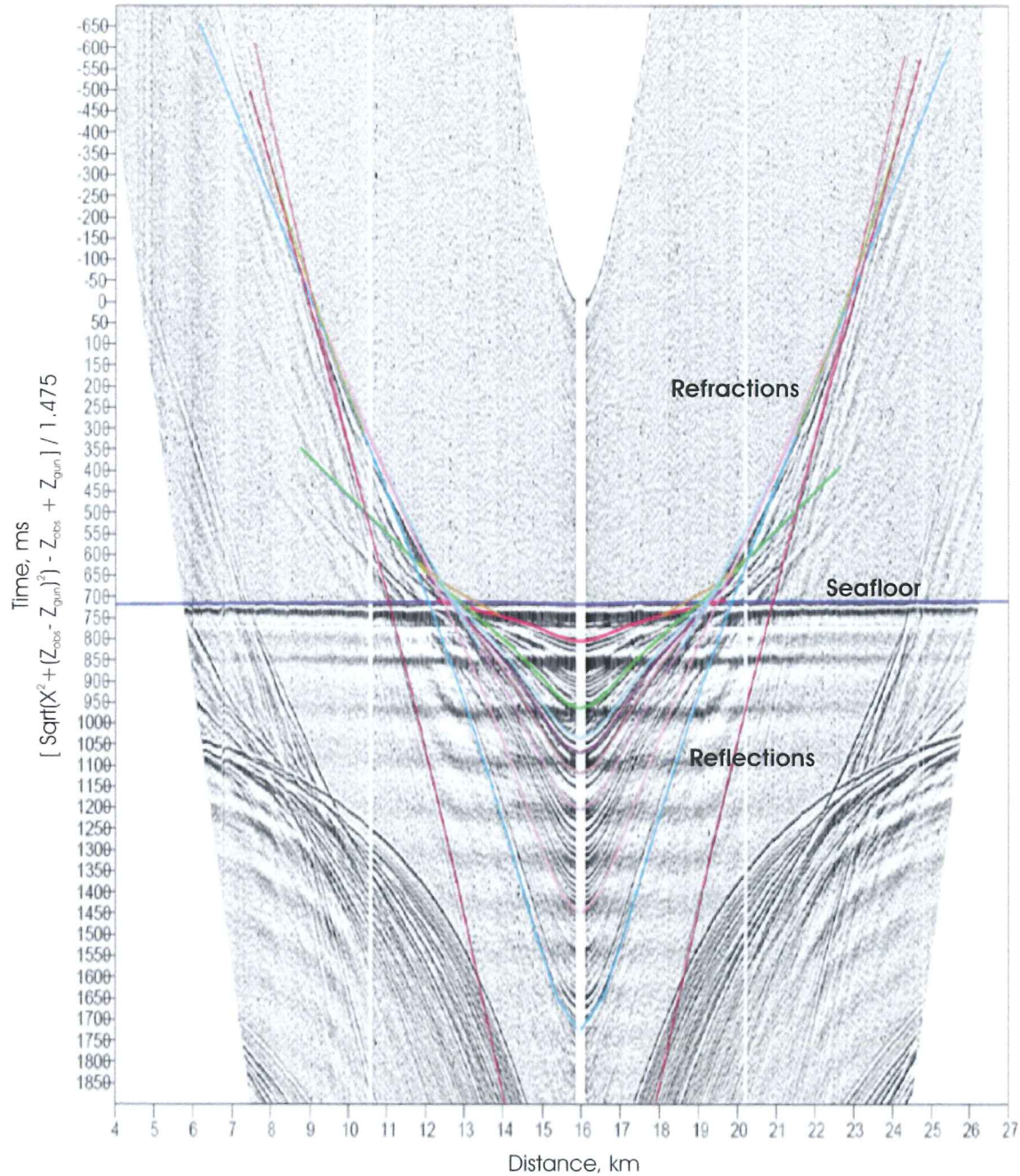


**Figure 4.1:** OBS A, channel 1 along Line 020. NMO correction was applied to the shot-gather to flatten the seafloor horizon, and to clearly display shallow reflections events. Refractions appear 'shallower' than the seafloor due to increased velocities at depth. (modified from Chian, 2008)

Chian's model is an amalgamation of the fitted travel time curves obtained from OBS A, OBS P, and OBS T at the study location. At five (5) positions along the survey, shown in Figure 4.2, model velocities and their corresponding depths were calculated in *Appendix A*. These five positions were chosen at, and adjacent to, the OBS position to develop an average gradient that was sensitive to lateral changes in depth of the  $p$ -wave velocity gradient. The resulting OBS velocity gradient is shown in Figure 4.3.

Depth-migrating the two seismic reflection profiles was necessary to determine the depth at which the BSR occurs at Sackville Spur. The approximation of hydrate concentration, achieved through the comparison of the averaged OBS gradient to those generated by Helgerud *et al.*'s (1999) hydrate model can only be achieved once the depth to the BSR is known. To depth-convert the two profiles, the OBS gradient was re-sampled at 100 m depth intervals to remove the effect of the hydrate and free gas, and ensure a more accurate migration over the remaining length of the profiles. The re-sampled velocities have been tabulated in *Appendix B*, and the gradient plotted in Figure 4.4.

The *Seiswide* software was used to apply the depth-migration. Restrictions associated with importing a velocity model into the software forced the selection of velocity layers. These layers could vary in thickness, however, each layer was limited to a constant velocity gradient. Layers were distinguished from one another by marked changes in the gradient, or slope of the curve, and are shown in Figure 4.4.

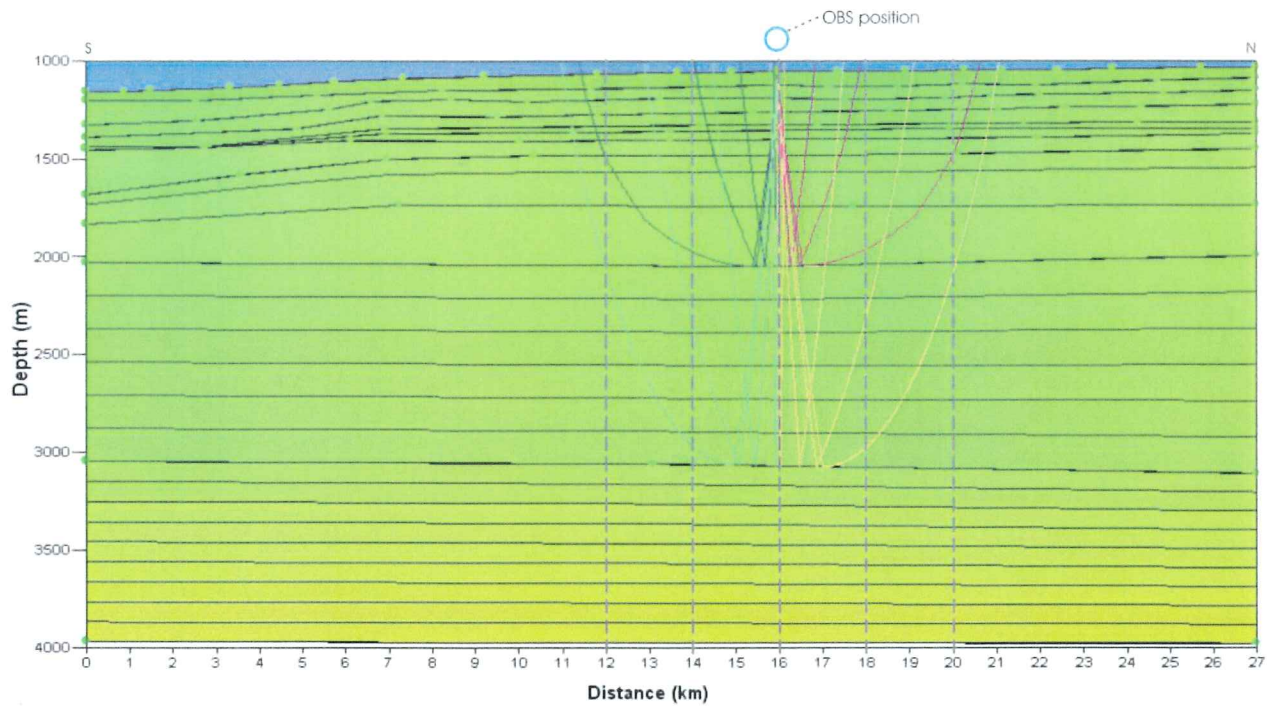


**Figure 4.2:** Chian's OBS velocity model, shown superimposed on Line 020. Velocity-depth data was extracted from five positions along the survey: 12km, 14km, 16km, 18km, and 20km to provide an average velocity gradient sensitive to minor depth variations of the model.

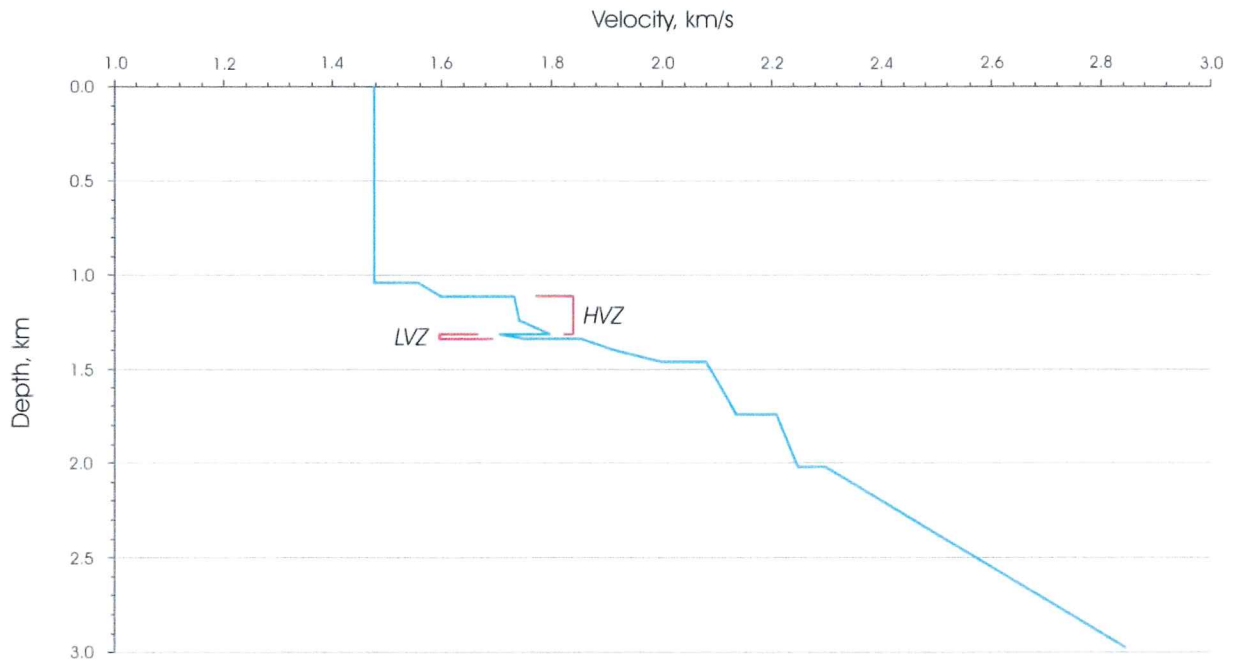


**Figure 4.3:** OBS velocity gradient from re-sampled Chian's model. The high-velocity zone (HVZ) represents inferred hydrate presence, and the low-velocity zone (LVZ) is attributed to free gas.

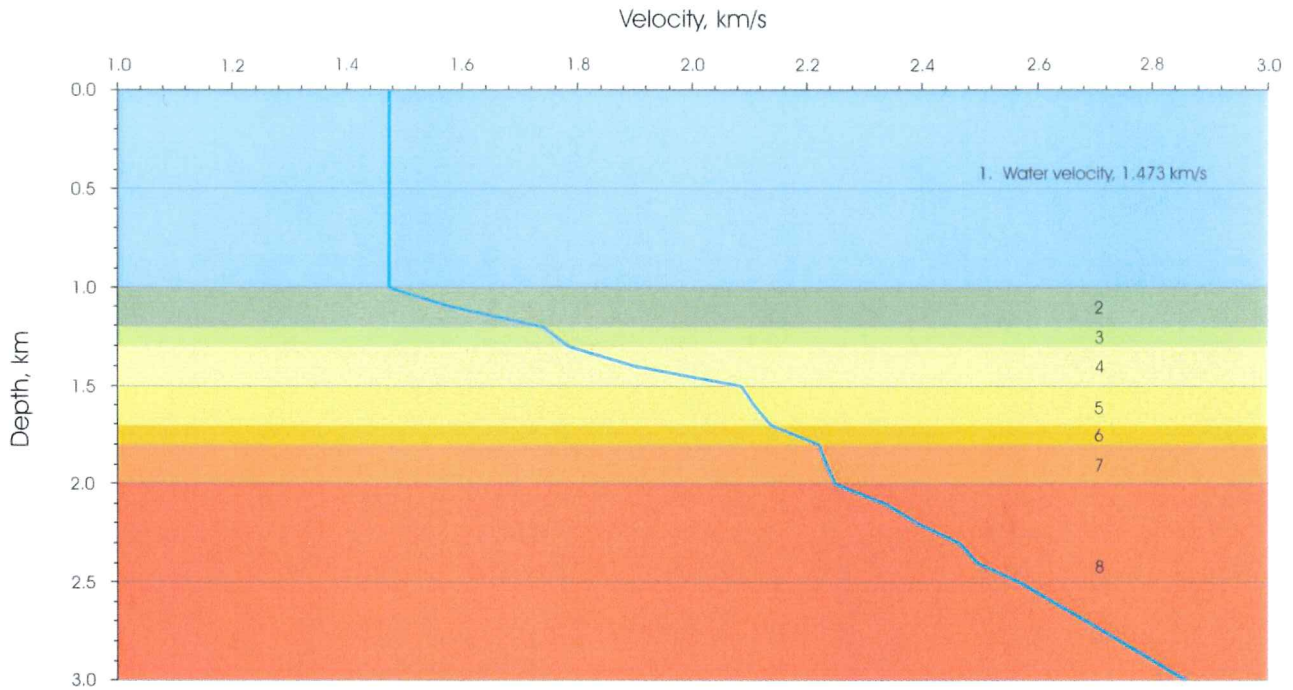


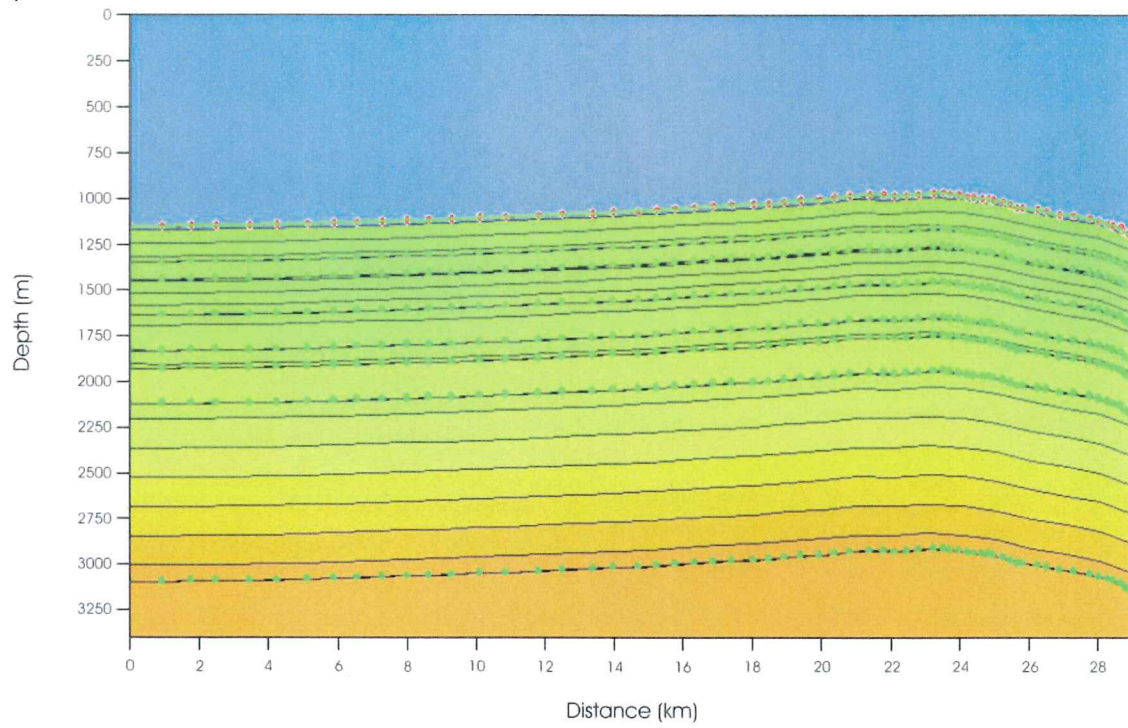
**Figure 4.4:** Average velocity gradient from OBS data, re-sampled at 100 m depth intervals. Eight (8) velocity layers were identified.

The velocity layers were input to the *SeisWide* software program in a way that each successive layer maintained the geometry of the seafloor reflector (Fig. 4.5). By applying the velocity model over the entire length of both reflection profiles in this manner, a number of key assumptions were made, including; 1) the assumption that sediment properties affecting *p*-wave velocities were laterally constant, thereby removing the need to correct interval velocities for changing water depths, and 2) the assumption that *p*-wave velocities varied uniformly with depth; a statement formulated on the basis of uniform compaction within the sediment column that would influence a systematic increase in density with depth.

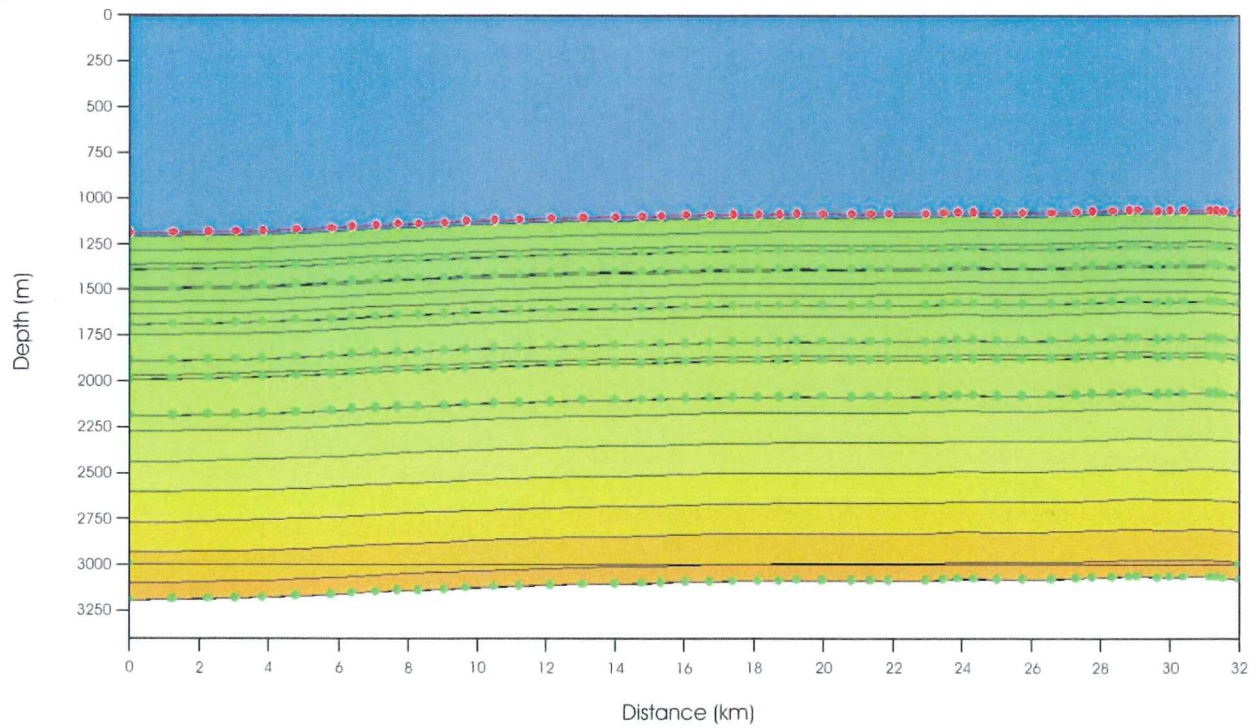
I was able to successfully apply the re-sampled velocity model to the TWT profiles of Line 020 and Line 021 to generate two depth-converted sections, displayed in

Figure 4.6. These depth sections are primitive, but provide a depth to the BSR that is likely accurate over this shallow interval, and necessary for determining hydrate concentrations.

(a)



(b)



**Figure 4.5:** Applied velocity model to (a) Line 021, and (b) Line 020. The velocity gradient was applied along the seafloor reflection horizon, and did not respect potential velocity changes associated with lithological variations with depth.

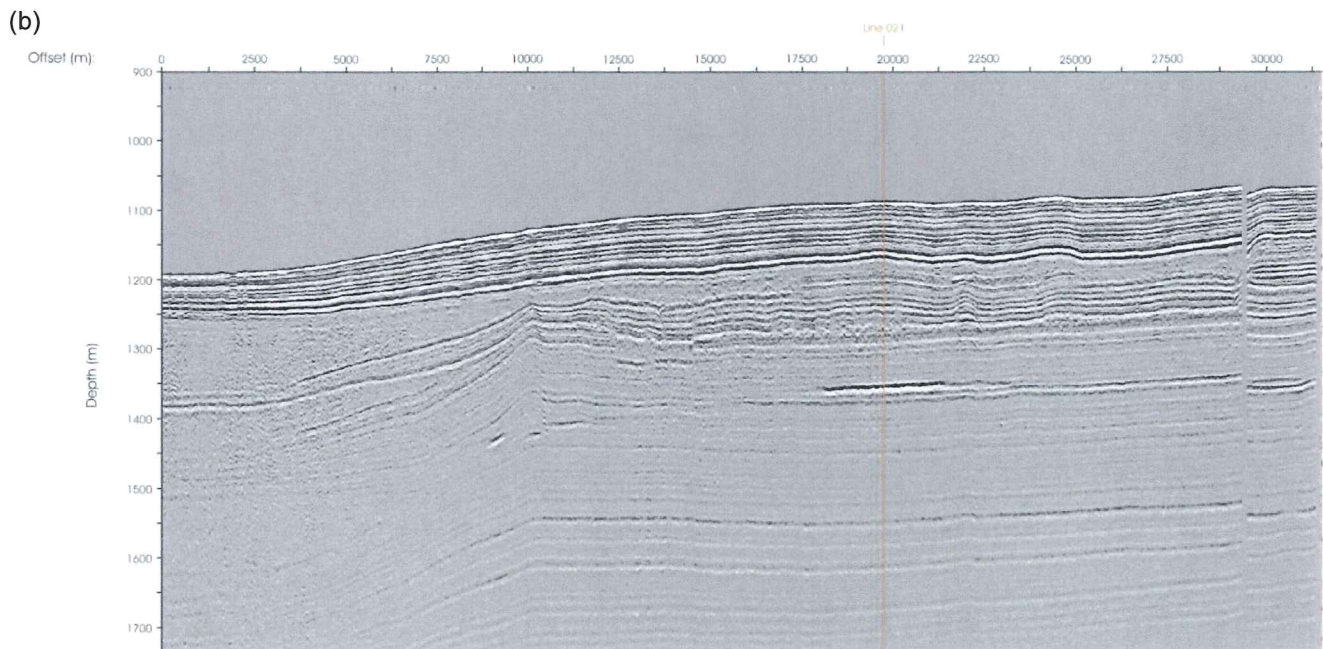
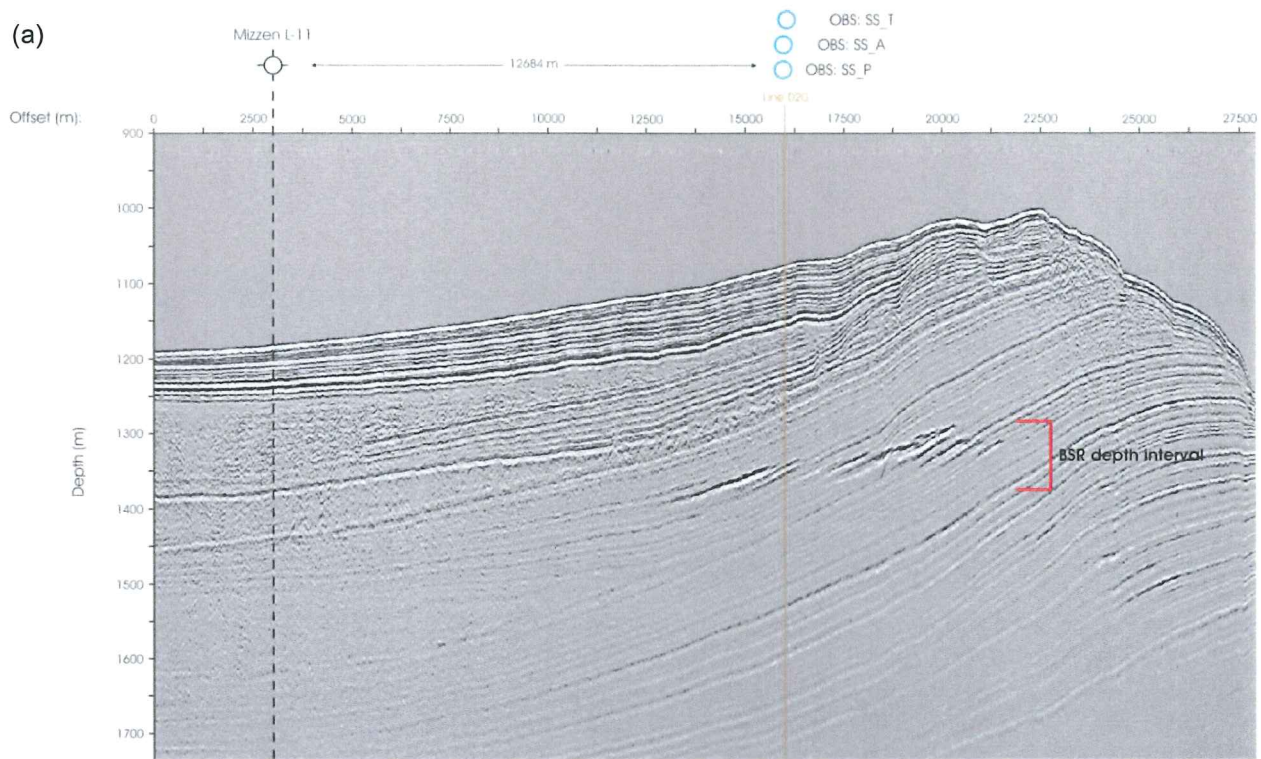
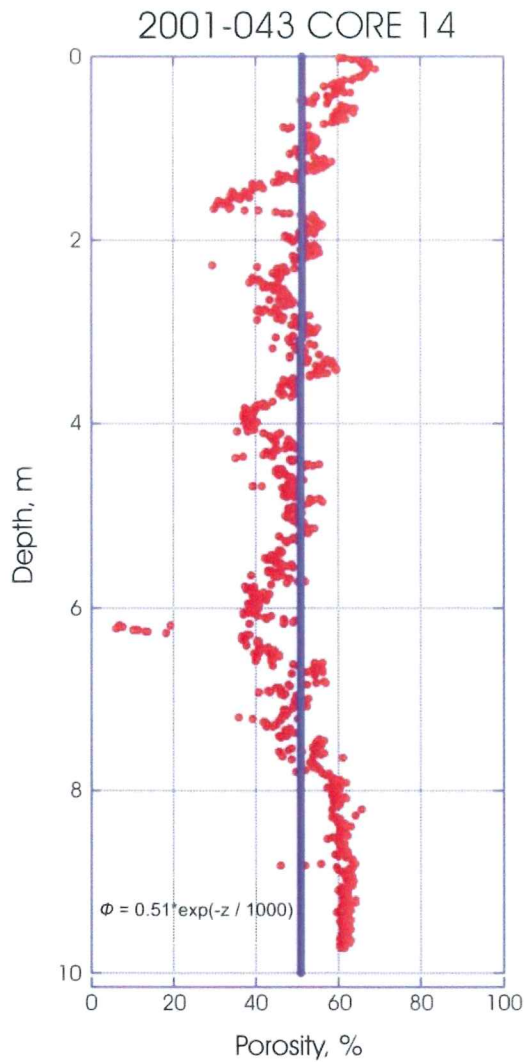


**Figure 4.6:** depth-converted seismic reflection profiles, (a) Line 021, (b) Line 020.

### 4.3 Piston Core Analysis

In order to interpret a seismic section in terms of gas hydrate volume, a relation between sediment porosity and  $p$ -wave velocity must be determined. We will use the effective medium model by Helgerud *et al.* (1999) to generate an approximation of the gas hydrate concentration at Sackville Spur. This model allows the hydrate to occur either within the pore fluid or as part of the solid frame, thereby reducing the overall sediment porosity. The model output is a  $p$ -wave velocity gradient at incremental hydrate concentrations. By comparing the effect of hydrate on the OBS velocity gradient to the hydrate concentration models, an estimation of hydrate volume at Sackville Spur can be formulated.

Physical property data from piston cores MD95-2026 and CORE 14 were used to provide mineralogical and porosity gradient approximations necessary for use in Helgerud *et al.*'s (1999) hydrate model. Velocity gradients characterized by varying hydrate concentrations were estimated using an effective medium model, assuming that porosities decrease smoothly with depth, following a standard exponential relationship:  $\Phi = \Phi_o \exp(-z / \lambda)$ , where  $\Phi_o = 0.51$ ,  $\lambda = 1000$  m and  $z =$  depth (m) below seafloor (Helgerud *et al.*, 1999; LeBlanc *et al.*, 2007). Sediment properties, derived from the MD95 core, were calculated to be an average mixture of 39% clay, 27% quartz, and 34% calcite (see *Table I*). Since clay and quartz have similar elastic properties, velocities are not sensitive to exact compositions (LeBlanc *et al.*, 2007). The porosity model for Sackville Spur was constrained to fit the measured porosities of CORE 14, resulting in a surficial porosity ( $\Phi_o$ ) value of approximately 51%. Figure 4.7 shows the CORE 14 porosity measurements, overlain by the fitted exponential porosity model.



	Sackville Spur	Scotia Margin
$\Phi_0$	0.51	0.60
$\lambda$ (m)	1000	1000
Clay (%)	39	85
Quartz (%)	27	15
Calcite (%)	34	0

**Table 1:** parameters for theoretical velocity model.  $\Phi = \Phi_0 \exp(-z / \lambda)$ , where  $\Phi_0$  is surface porosity and  $\lambda$  the exponential decay factor. Compared to the Scotia Margin, a marked change in sediment mineralogy is evident.

**Figure 4.7:** CORE 14 porosity data, fitted with exponential porosity gradient model from Helgerud et al. (1999). The above porosity gradient may appear non-exponential, however, at depths far exceeding 10 m, the exponential behaviour of the curve is more apparent.

## CHAPTER 5: RESULTS

The depth-migrated reflection profiles (Fig. 4.6) display a prominent BSR at depths ranging from 1280 m – 1400 m below sea level (mbsl) at the OBS location. This depth range correlates well with the velocity anomaly identified in Chian's OBS model, shown in Figure 4.3. At 1327 m depth, a sharp decrease in velocity from 1800 m/s to 1700 m/s has been calculated from the ray-tracing analysis, and is attributed to the presence of a free gas zone. The free gas zone is estimated to be approximately 28 m thick, as suggested from the LVZ captured in Chian's model.

Inferred hydrate presence at Sackville Spur is supported by a marked velocity increase to 1730 m/s at 1130 m depth. Anomalously high velocities, relative to the average OBS gradient, are characteristic indicators of hydrate presence in ocean bottom sediment. The velocity inversion imaged by Chian's OBS model displays a subsurface BSR signature similar to that described by Figure 3.4 (a), where free gas existing beneath hydrate-bound sediment has caused an acoustic phase reversal.

To compare the effect of hydrate on the OBS velocity gradient, hydrate concentration curves derived from Helgerud *et al.*'s (1999) model have been plotted with the OBS gradient in Figure 5.1 as velocity vs. depth below sea level. The hydrate effect on the OBS velocity gradient would suggest possible hydrate concentrations up to 9%. The difference in depth between the top of the HVZ at 1130 m, and the top of the low-velocity free gas zone at 1327 m, would suggest a GHSZ of nearly 200 m thickness. However, it is suggested that the thickness of the GHSZ is likely inaccurate, as OBS data resolutions contain an inherent coarseness that limits the accuracy of the model.

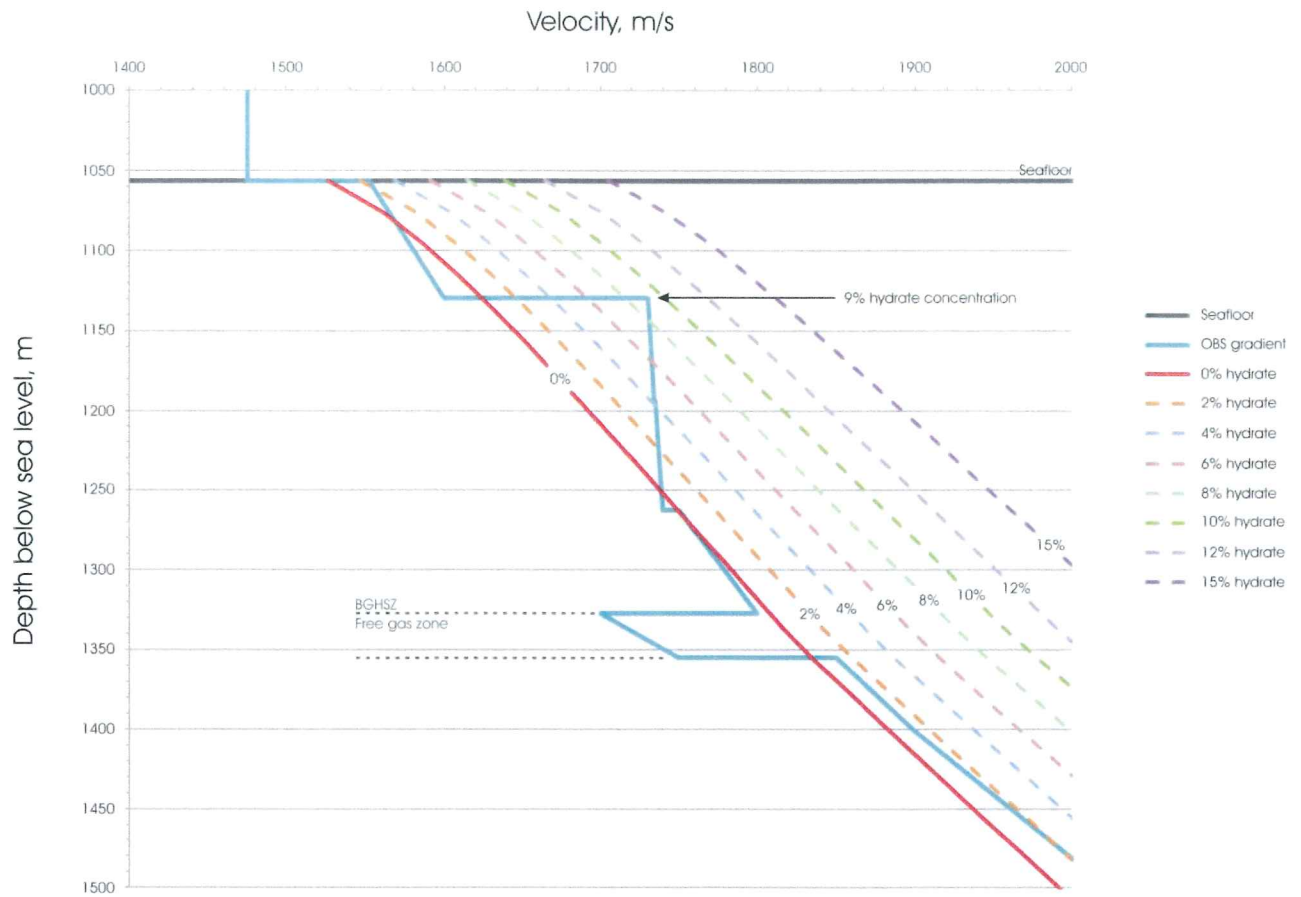


**Figure 5.1:** OBS velocity comparison to hydrate concentration curves generated from Helgerud et al., (1999). Hydrate concentration curves were repositioned in depth to begin at the seafloor, and in velocity so that the 0% hydrate curve overlapped the trend of the average OBS gradient devoid of hydrate or gas. The HVZ, caused by inferred hydrate presence, is suspected to reach concentrations of 9%.

## CHAPTER 6: DISCUSSION

### 6.1 Velocity Model & Depth Sections

Initial investigation into depth variations along the two seismic reflection profiles was achieved by applying Chian's 1-D velocity-depth model to each of the 2-D reflection profiles. The model was depth-averaged at five positions laterally adjacent to the OBS, and later velocity-averaged to remove the effect of inferred hydrate and free gas zones for entry into the *Seiswide* software. The resulting depth-converted sections, shown in *Figure 4.6*, provide a modest approximation of the depth of the BSR at Sackville Spur. However, lateral  $p$ -wave variations are poorly constrained by this method, as it fails to compensate for changes in both depth to the seafloor, and differences in physical property characteristics of subsurface lithologies. Additional model shortcomings (e.g. resolution) are associated with the ray-tracing process by which velocity information is extracted from the OBS data. In being constrained primarily by the move-out of the reflected and refracted arrivals recorded by the OBS, Chian's velocity model contains inherent error associated with user-picked move-out velocities; especially at depth where reflection energies become weak due to spherical spreading, among other factors. Therefore, the velocity model and consequent depth profiles may not be justified at far offsets from the OBS position, or at depths  $>1500$  m. To develop a model more sensitive to lateral velocity variations, additional data would be required from several OBS along the length of each profile.

Wireline log data from the Mizzen L-11 well was also anticipated to strengthen the OBS model at depth. A sonic log is an acoustic log that relates travel time of  $p$ -waves versus depth, commonly measured in  $\mu\text{s}/\text{m}$ . A simple calculation can therefore

provide a velocity estimate, in m/s, that was expected to increase the accuracy of the OBS model with depth. However, after examination, the associated sonic log displays no logical trend, and was deemed an ineffective supporting estimate of velocity at Sackville Spur.

## 6.2 Comparison of Porosity Models & Gas Hydrate Concentrations

The porosity model was developed by curve-fitting an exponential porosity equation developed by Helgerud *et al.* (1999) to CORE 14 physical property data, shown in Figure 4.7. Sediment property derived from density measurements were acquired via the multi-sensor track analyses, and justified with constant volume discrete sample analyses. Modification of the Helgerud *et al.* (1999) model to best approximate the piston core data was minimal, and included only a minor recalculation of surficial porosity related to those values measured at Sackville Spur. A shift of the curve from 60% surficial porosity on the Scotia Margin to 51% at Sackville Spur provided an accurate model sensitive to the CORE 14 data. Changes to the exponential decay factor,  $\lambda$ , were decidedly unnecessary due to zero data control associated with fitting the porosity model to unknown sediment property data at depths greater than those provided in the piston core.

Two neutron porosity (NPOR) logs from the Mizzen well were examined to provide a more accurate approximation of porosity at depth. NPOR logs estimate porosity by relating the difference in neutrons received at the tool from those initially emitted to the amount of hydrogen located primarily in the pore fluids of the rock or sediment. In the first log, initial measurements displayed porosity values similar to

those calculated in piston core; however, a) no trend with depth was evident, and b) the log interval began too deep (at approximately 1700 m depth), thereby failing to capture relevant porosity data representative of the actual spur deposit. A LWD resistivity curve was examined for potential to approximate subsurface porosities. It confirmed the porosity trend applied to the piston core data. Derivation of porosity from resistivity requires some assumptions of values input to the application of Archie's Law. Although the absolute values of porosity may be in error, the near vertical trend in porosity versus depth, derived from piston core data, can be confirmed.

The hydrate concentration models shown in Figure 5.1 suggest bulk hydrate concentrations of 9% at Sackville Spur. Similar models applied to Scotia Margin sediments yielded estimated hydrate concentration values of ~2 – 6%, and ~8 – 15% for the Blake Ridge (LeBlanc *et al.*, 2007). It is noted that these results differ by factors of 0.22 – 0.66, and 0.88 – 1.66, respectively, when compared to Sackville Spur. Preliminary hydrate volume estimates compiled by Majorowicz and Osadetz (1993) on the Atlantic margin were done with an inferred mean thickness of 79 m. Therefore, primitive hydrate volume estimates of  $1.12 \times 10^9 \text{ m}^3$  at Sackville Spur can be derived from an average porosity of 9%, a GHSZ thickness of 79 m and a BSR area of  $156 \text{ km}^2$ . The suggested thickness of the GHSZ at nearly 200 m, as indicated from Chain's OBS velocity model (Fig. 5.1), was not considered in the hydrate volume estimate calculation. The OBS model contained an inherent coarseness that was presumed to likely have a substantial negative effect on the accuracy of the estimate. Therefore, the average GHSZ thickness on the Atlantic margin is thought to represent a low-end approximation of hydrate volume in the case of Sackville Spur.

Mineralogical variations, shown in *Table 1*, may provide an explanation for differences in hydrate concentration at Sackville Spur when compared to the Scotia Margin. High calcite estimates, due in part to an abundance of fossil material observed in the MD95-2026 core, may account for high porosities and consequently relative higher hydrate concentrations at the spur. Continued sedimentation on top of the carbonate-rich deposit may have had a decreased effect on compaction when compared to other regions of decreased relative carbonate content. The preservation of pore space by fossil shells at Sackville Spur may have provided additional volumes in which hydrate could occupy.

The nature of contourite deposition itself also provides a possible explanation for greater hydrate concentration estimates at Sackville Spur than on the Scotia Margin. The shale-rich Scotia slope is dominated by debris flow and mass-wasting deposit types that are not heavily influenced by ocean current circulation (LeBlanc *et al.*, 2007). An increased current velocity regime at Sackville Spur may influence water column energies large enough to limit the widespread sedimentation of clay minerals, as supported by Viana and Rebesco (2007). In such an environment, the overall potential for pore volumes to become occupied, or 'clogged' by this finer clay fraction would be significantly reduced.

## CHAPTER 7: CONCLUSIONS

Continental margins represent a vast potential for storing methane gas in the form of crystalline gas hydrate. Two wide-angle reflection seismic survey lines were examined along the eastern margin of the Grand Banks at Sackville Spur after the inferred occurrence of methane hydrate was determined from a subsurface BSR, totalling an area approximately 156 km<sup>2</sup> in size. The dipping BSR displays a series of high-amplitude, phase-reversed reflection events at depths of 1280 – 1400 mbsl, consistent with the OBS velocity model that has captured velocity inversions attributed to free gas trapped beneath hydrate-bound sediment. Approximate sediment mineralogy characteristics of Sackville Spur were derived from piston core analyses. A suggested mixture of 39% clay, 27% quartz and 34% calcite forms the assumed bulk mineralogy of the contourite deposit at Sackville Spur.

Application of hydrate concentration models of Helgerud *et al.* (1999) provided an approximation of 9% hydrate concentration within the GHSZ. High carbonate mineralogy and a decreased clay fraction at the spur deposit justify a larger hydrate concentration than that of ~2 – 8% approximated along the Scotia Margin. Primitive estimates based on inferred GHSZ thicknesses identified in studies by Majorowicz and Osadetz (1993) along the Atlantic Margin indicate roughly  $1.12 \times 10^9$  m<sup>3</sup> of natural gas hydrate at Sackville Spur. What is most important in this estimate is the concentration potential of methane in hydrate achieving up to 160 times greater masses (per equivalent volume) than natural gas in conventional reservoirs.

## REFERENCES

- Bil, K.J., 2000. Economic Perspective of Methane from Hydrate, *in*: Max, M.D. (ed.), *Natural Gas Hydrate in Oceanic and Permafrost Environments*, Kluwer Academic Publishers, p. 349-360.
- Campbell, D.C., Piper, D.J.W., Douglas, E.V. and Migeon, S., 2002. Surficial geology of Flemish Pass: Assessment of hazards and constraints to development. Geological Survey of Canada Open File 1454.
- Chian, D., 2008. Hud2004-024 Ocean Bottom Seismometer Data Analysis: Sackville Spur Bottom Simulating Reflector (BSR), Unpublished report to Geological Society of Canada – Atlantic, Dartmouth, NS (D. Mosher)..
- Dallimore, S.R. and Collett, T.S. (eds.), 2005. Scientific Results from the Mallik 2002 Gas Hydrate Production Research Well Program, Mackenzie Delta, Northwest Territories, Canada. *Geological Survey of Canada, Bulletin 585*.
- Deptuck, M.E., Mosher, D.C., Campbell, D.C., Hughes-Clarke, J.E., & Noseworthy, D., 2007. Along slope variations in mass failures and relationships to major Plio-Pleistocene morphological elements, SW Labrador Sea. *Submarine Mass Movements and Their Consequences*, p. 37-45.
- Dickens, G.R., 2000. Modeling the Global Carbon Cycle With a Gas Hydrate Capacitor: Significance for the Latest Paleocene Thermal Maximum, *in*: Paull, C.K., and Dillon, W.P. (eds.), *Natural Gas Hydrates: Occurrence, Distribution, and Detection*, *Geophysical Monograph*, p. 19-38.
- Dillon, W.P. and Max, M.D., 2000. Oceanic Gas Hydrate, *in*: Max, M.D. (ed.), *Natural Gas Hydrate in Oceanic and Permafrost Environments*, Kluwer Academic Publishers, p. 61-76
- Dyke, A.S., Andrews, J.T., Clark, P.U., England, J.H., Miller, G.H., Shaw, J., and Veillette, J.J., 2002. The Laurentide and Innuitian ice sheets during the Last Glacial Maximum, *Quaternary Science Reviews*, v. 21, p. 9-31.
- Faugères, J.-C. and Stow, D.A.V., 2008. Contourite Drifts: Nature, Evolution and Controls, *in*: Rebesco, M. and Camerlenghi, A. (eds.), *Contourites, Developments in Sedimentology*, v. 60.
- Gay, A., Lopez, M., Cochonat, P., Sultan, N., Cauquil, E. and Brigaud, F., 2003. Sinuous pockmark belt as indicator of a shallow buried turbiditic channel on the lower slope of the Congo basin, West African margin, *in*: Van Rensbergen, P., Hillis, R.R., Maltman, A.J. and Morley, C.K. (eds.), *Subsurface Sediment Mobilization*, *Geological Society of London, Special Publication 216*, p. 173-189.
- Helgerud, M.B., Dvorkin, J., Nur, A., Sakai, A. and Collett, T., 1999. Elastic-wave velocity in marine sediments with gas hydrates: Effective medium modeling. *Geophysical Research Letters*, v. 26, n. 13, p.2021-2024.
- Hesse, R., 1990. Pore water anomalies in gas hydrate-bearing sediments of the deeper continental margins: Facts and Problems. *J. Inclusion Phenomena and Molecular Recognition in Chemistry*, 8, p.117-138.
- Huppertz, T.J. and Piper, D.J.W., 2009. The influence of shelf-crossing glaciation on continental slope sedimentation, Flemish Pass, eastern Canadian continental margin, *Marine Geology*, v. 265, p. 67-85.
- Kennard, L., Schafer, C., and Carter, L., 1990. Late Cenozoic evolution of Sackville Spur: a sediment drift on the Newfoundland continental slope, *Canadian Journal of Earth Sciences*, v. 27, p. 863-878.

- King, L.H., Fader, G.B., Poole, W.H. and Wanless, R.K., 1985. Geological setting and age of the Flemish Cap granodiorite, east of the Grand Banks of Newfoundland. *Canadian Journal of Earth Sciences*, v. 22, p.1286-1298.
- Kvenvolden, K.A. and Lorenson, T.D., 2001. The Global Occurrence of Natural Gas Hydrate, *in*: Paull, C.K., and Dillon, W.P. (eds.), *Natural Gas Hydrates: Occurrence, Distribution, and Detection, Geophysical Monograph 124*, p.3-18.
- Laberg, J.S., Vorren, T.O., 1995. Late Weichselian submarine debris flow deposits on the Bear Island Trough Mouth Fan, *Marine Geology*, 127 (1–4), p. 45–72.
- LeBlanc, C., Loudon, K., and Mosher, D., 2007. Gas hydrates off Eastern Canada: Velocity models from wide-angle seismic profiles on the Scotian Slope, *Marine and Petroleum Geology* 24, p. 321-335.
- LeBlanc, C.R. 2002. Central Scotian Slope Stability: the possible role of gas hydrates. B.Sc. thesis, Department of Earth Sciences, Dalhousie university, Halifax, N.S..
- Majorowicz, J.A. and Osadetz, K.G., 2003. Natural gas Hydrate Stability in the East Coast Offshore-Canada. *Natural Resources Research*, 12, n. 2, p. 93-104.
- Majorowicz, J.A. and Osadetz, K.G., 1993. Gas hydrate distribution and volume in Canada. *American Association of Petroleum Geologists Bulletin*, 85, p. 1211-1230.
- Max, M.D., 2000. Hydrate Resource, Methane Fuel, and a Gas-Based Economy?, *in*: Max, M.D. (ed.), *Natural Gas Hydrate in Oceanic and Permafrost Environments*, Kluwer Academic Publishers, p.361-370.
- McConnell, D.R., and Kendall, B.A., 2002. Images of the Base of Gas Hydrate Stability, Northwest Walker Ridge, Gulf of Mexico. *Offshore Technology Conference (OTC) 14104*, Houston, Texas, USA, May 2002.
- Mosher, D.C., 2008. Bottom simulating reflectors on Canada's East Coast margin: Evidence for gas hydrate. Proceedings of the 6<sup>th</sup> International Conference on Gas Hydrates (ICGH 2008), Vancouver, British Columbia, CANADA, July 6-10, 2008.
- Ondréas, H., Olu, K., Fouquet, Y., Charlou, J.L., Gay, A., Dennielou, B., Donval, J.P., Fifis, A., Nadalig, T., Cochonat, P., Cauquil, E., Bourillet, J.F., Le Moigne, M., and Sibuet, M., 2005. ROV study of a giant pockmark on the Gabon continental margin, *Geo-Mar Lett*, 25, p. 281-292.
- Paull, C.K., Matsumoto, R., and Wallace, P., 1996. *Proc. Ocean Drilling program, Initial Report*, 164, p. 623.
- Piper, D.J.W., 2005. Late Cenozoic evolution of the continental margin of eastern Canada, *Norwegian Journal of Geology*, v. 85, p. 305-318.
- Piper, D.J.W. and Campbell, D.C., 2005. Quaternary geology of Flemish Pass and its application to geohazard evaluation for hydrocarbon development. *GAC Special Paper 43*, p. 29-43.
- Rebesco, M., Camerlenghi, A. and Van Loon, A.J., 2008. Contourite Research: A field in full development, *in*: Rebesco, M. and Camerlenghi, A. (eds.), *Contourites, Developments in Sedimentology*, v. 60.
- Riedel, M., Spence, G.D., Chapman, N.R. and Hyndman, R.D., 2002. Seismic investigation of a vent field

- associated with gas hydrates, offshore Vancouver Island. *Journal of Geophysical Research*, v. 107, n. B9.
- Sloan, E.D. and Koh, C.A.. Clathrate Hydrates of Natural Gases, Third Edition, CRC Press, 2008: Boca Raton, Florida.
- Stea, R.R., Piper, D.J.W., Fader, G.B.J., and Boyd, R., 1998. Wisconsinan glacial and sea-level history of Maritime Canada and the adjacent continental shelf: A correlation of land and sea events. *GSA Bulletin*, v.110, no.7, p.821-845.
- Stow, D.A.V., Faugères, J.-C., Howe, J.A., Pudsey, C.J. and Viana, A.R., 2002. Bottom currents, contourites and deep-sea sediment drifts: current state-of-the-art, *in*: Stow, D.A.V., Pudsey, C.J., Howe, J.A., Faugères, J.-C. and Viana, A.R. (eds.), *Deep-Water Contourite Systems: Modern Drifts and Ancient Series, Seismic and Sedimentary Characteristics. Geological Society, London, Memoirs*, 22, p. 7-20.
- Suess, E., Torres, M.E., Bohrmann, G., Collier, R.W., Rickert, D., Goldfinger, C., Linke, P., Heuser, A., Sahling, H., Heeschen, K., Jung, C., Nakamura, K., Greinert, J., Pfannkuche, O., Trehu, A., Klinkhammer, G., Whiticar, M.J., Eisenhauer, A., Teichert, B., and elvert, M., 2001. Sea Floor Methane Hydrates as Hydrate Ridge, Cascadia Margin, *in*: Paull, C.K., and Dillon, W.P. (eds.), *Natural Gas Hydrates: Occurrence, Distribution, and Detection, Geophysical Monograph 124*, p.87-98.
- Taylor, A., Weitmiller, R. and Judge, A., 1979. Two risks to drilling and production off the east coast of Canada-earthquakes and gas hydrates, *in*: Denver, W. (ed.), *Proc. Symposium Research on the Labrador Coastal and Offshore Region: Memorial University, Newfoundland*, p. 91–105.
- Tucholke, B.E. and Bryan, G.M., 1977. Gas-hydrate horizons detected in seismic-profiler data from the western north Atlantic. *American Association of Petroleum Geologists Bulletin* 61, p.698-707.
- Viana, A.R., Almeida JR., W., Nunes, M.C.V., and Bulhões, E.M., 2007. The economic importance of contourites, *in*: Viana, A.R. and Rebesco, M. (eds.), *Economic and Palaeoceanographic Significance of Contourite Deposits, Geological Society*, n.276, p.1-24.
- Warnke, D.A., 1970. Glacial erosion, ice rafting and glacial-marine sediments: Antarctica and the southern ocean, *American Journal of Science*, 269, p. 276–294.
- Xu, X.-Y. and Ruppel, C., 1999. Predicting the occurrence, distribution and evolution of methane gas hydrate in porous marine sediments. *Journal of Geophysical Research*, v. 104, p. 5081-5095.

## APPENDIX A

*Velocity-depth data extracted from Chian's OBS model at five positions along Line 020*

DISTANCE									
12 km		14 km		16 km		18 km		20 km	
Depth, km	Velocity, km/s								
0	1.472	0	1.473	0	1.473	0	1.473	0	1.474
1.066	1.475	1.058	1.475	1.055	1.475	1.055	1.475	1.048	1.475
1.066	1.552	1.058	1.552	1.055	1.552	1.055	1.552	1.048	1.552
1.14	1.6	1.132	1.6	1.124	1.6	1.133	1.6	1.121	1.6
1.14	1.73	1.132	1.73	1.124	1.73	1.133	1.73	1.121	1.73
1.199	1.734	1.193	1.734	1.192	1.734	1.196	1.734	1.189	1.734
1.199	1.735	1.193	1.735	1.192	1.735	1.196	1.735	1.189	1.735
1.273	1.74	1.268	1.74	1.262	1.74	1.258	1.74	1.251	1.74
1.273	1.75	1.268	1.75	1.262	1.75	1.258	1.75	1.251	1.75
1.335	1.8	1.329	1.8	1.326	1.8	1.323	1.8	1.322	1.8
1.335	1.7	1.329	1.7	1.326	1.7	1.323	1.7	1.322	1.7
1.364	1.75	1.36	1.75	1.355	1.75	1.351	1.75	1.346	1.75
1.364	1.85	1.36	1.85	1.355	1.85	1.351	1.85	1.346	1.85
1.407	1.9	1.404	1.9	1.401	1.9	1.399	1.9	1.396	1.9
1.407	1.9	1.404	1.9	1.401	1.9	1.399	1.9	1.396	1.9
1.484	2.0	1.485	2.0	1.485	2.0	1.479	2.0	1.474	2.0
1.484	2.08	1.485	2.08	1.485	2.08	1.479	2.08	1.474	2.08
1.74	2.14	1.741	2.14	1.742	2.14	1.743	2.14	1.741	2.14
1.74	2.21	1.741	2.21	1.742	2.21	1.743	2.21	1.741	2.21
2.045	2.25	2.047	2.25	2.049	2.25	2.039	2.25	2.029	2.25
2.045	2.3	2.047	2.3	2.049	2.3	2.039	2.3	2.029	2.3
3.059	2.9	3.064	2.9	3.071	2.9	3.078	2.9	3.084	2.9
3.059	3.2	3.064	3.2	3.071	3.2	3.078	3.2	3.084	3.2
3.975	4.1	3.976	4.1	3.977	4.1	3.977	4.1	3.978	4.1

## APPENDIX B

*Re-sampled OBS velocities at 100 m intervals, with velocity layers.*

Distance	12km	14km	16km	18km	20km		
Depth, km	Velocity, km/s	Velocity, km/s	Velocity, km/s	Velocity, km/s	Velocity, km/s	Ave. velocity, km/s	Layer #
0	1.472	1.473	1.473	1.473	1.474	1.473	1 - water
1	1.473	1.475	1.475	1.475	1.475	1.4746	2
1.1	1.575	1.58	1.58	1.58	1.585	1.58	
1.2	1.74	1.74	1.735	1.74	1.74	1.739	3
1.3	1.78	1.785	1.78	1.79	1.785	1.784	4
1.4	1.895	1.9	1.9	1.9	1.9	1.899	5
1.5	2.08	2.085	2.085	2.085	2.09	2.085	
1.6	2.11	2.11	2.105	2.105	2.115	2.109	
1.7	2.14	2.13	2.14	2.135	2.14	2.137	6
1.8	2.22	2.22	2.22	2.22	2.22	2.22	7
1.9	2.23	2.23	2.24	2.235	2.235	2.234	
2	2.25	2.245	2.25	2.25	2.25	2.249	8
2.1	2.34	2.33	2.325	2.34	2.345	2.336	
2.2	2.39	2.39	2.385	2.395	2.4	2.392	
2.3	2.51	2.45	2.45	2.45	2.45	2.462	
2.4	2.45	2.505	2.5	2.505	2.515	2.495	
2.5	2.575	2.565	2.57	2.56	2.565	2.567	
2.6	2.625	2.63	2.625	2.625	2.625	2.626	
2.7	2.695	2.685	2.68	2.69	2.68	2.686	
2.8	2.75	2.74	2.745	2.74	2.74	2.743	
2.9	2.82	2.8	2.8	2.8	2.795	2.803	
3	2.865	2.86	2.855	2.855	2.85	2.857	